`

Effect of Gamma-Rays on Morphology and Tensile Properties of Polypropylene Fiber for Cement Composites.

by

Sanchay Sushil Tiwari

A Thesis Presented in Partial Fulfillment
of the Requirements for the Degree
Master of Science

Approved April 2018 by the
Graduate Supervisory Committee:

Barzin Mobasher, Co-Chair
Narayanan Neithalath, Co-Chair
Subramaniam Dharmarajan
Keith Holbert

ARIZONA STATE UNIVERSITY

May 2018

`

ABSTRACT

Concrete is relatively brittle, and its tensile strength is typically only about one-tenth of its compressive strength. Regular concrete is therefore normally uses reinforcement steel bars to increase the tensile strength. It is becoming increasingly popular to use random distributed fibers as reinforcement and polymeric fibers is once such kind. In the case of polymeric fibers, due to hydrophobicity and lack of any chemical bond between the fiber and matrix, the weak interface zone limits the ability of the fibers to effectively carry the load that is on the matrix phase. Depending on the fiber's surface asperity, shape, chemical nature, and mechanical bond characteristic of the load transfer between matrix and fiber can be altered so that the final composite can be improved. These modifications can be carried out by means of thermal treatment, mechanical surface modifications, or chemical changes The objective of this study is to measure and document the effect of gamma ray irradiation on the mechanical properties of macro polymeric fibers. The objective is to determine the mechanical properties of macro-synthetic fibers and develop guidelines for treatment and characterization that allow for potential positive changes due to exposure to irradiation. Fibers are exposed to various levels of ionizing radiation and the tensile, interface and performance in a mortar matrix are documented. Uniaxial tensile tests were performed on irradiated fibers to study fiber strength and failure pattern. SEM tests were carried out in order to study the surface characteristic and effect of different radiation dose on polymeric fiber. The interaction of the irradiated fiber with the cement composite was studied by a series of quasi-static pullout test for a specific embedded length. As a final task, flexural tests were carried out for different irradiated fibers to sum up the

`

investigation. An average increase of 13% in the stiffness of the fiber was observed for 5 kGy of radiation. Flexural tests showed an average increase of 181% in the Req3 value and 102 % in the toughness of the sample was observed for 5 kGy of dose.

`

To Maa and Papa,

I cannot describe how blessed I am to have such supporting parents in my life.

`

ACKNOWLEDGMENTS

Foremost, I would like to express my sincere gratitude to my advisor Dr. Barzin Mobasher for letting me work and for providing me such great research opportunities. The constant motivation and patience he has given me helped me to stay focused in my work. His valuable insight has helped me to develop and grow. I also want to extend my appreciation to Dr. Subramanian D. Rajan, Dr. Keith Holbert and Dr. Narayanan Neithalath who served as my committee members, helping and supervising my progress in Master's degree program.

I would also like to thank Dr. Yiming Yao who taught me almost every basic skills including preparing and conducting experiment, data analysis. Dr. Yiming Yao's mentorship helped me gauge many complex ideas which he simplified for me paving a straightforward path for my work. I would like to sincerely thank Farrokh Kianmofard and Vinodh Vijayasarthy for their immense help in all the experimental work under my project. I also appreciate the assistance provided by Mr. Peter Goguen and Mr. Jeff Long for all their help in the laboratory.

I would also like to thank my professor, Dr. H.B.Dhonde and Dr. Milinda Mahajan for their enthusiasm in my work and guidance. I extend my heartfelt gratitude to my friends – Dhruvil Shah, Rushabh Talati, Samarth Shah, Deep Shah and Sayali Joshi for providing me with the moral support and also my brother-Sourabh Tiwari and my dear grandparents for their constant support.

`

Lastly, I would like to thank my mother, Sarita Tiwari for showing faith in me and motivating me to achive my goals. I would like to thank my Dad, Sushil Tiwari, because of whom I looked forward to this discipline.

`

TABLE OF CONTENT

Page

`

CHAPTER Page

`

LIST OF FIGURES

Figure Page

`

Figure Page

`

Figure Page

`

Figure Page

`

LIST OF TABLES

Table Page

`

1 INTRODUCTION AND LITERATURE REVIEW

1.1 Introduction and Statement of the problem:

Cement-based materials are used extensively in a wide range of construction projects. Despite their high compressive strength however, these materials have a low tensile strength and toughness. For elements that undergo general tensile loading, reinforcement is required to improve the tensile and flexural performance, and that may be supplied by short fibers in order to improve the sustainability and performance of the final product. Reinforcing concrete with macro synthetic fibers has a history of more than 40 years [1] [2] [3] [4], yet there is a growing area of opportunity to utilize the strength and stiffness of fibers in structural applications for serviceability and also minimum reinforcement. Macro synthetic, alkali resistant glass, and steel fibers each have their own properties and features.

Steel fibers provide high levels of strength and toughening, however due to their bond strength, their effectiveness is observed after the matrix has fully cracked. Glass fibers suffer from long term durability, however macro synthetic fibers are 100% alkali resistant and have high resistance to corrosion when compared with steel fibers and long term aging when compared with glass fibers. Composite materials consists of two phases of matrix and fibers, however these two phases interact by means of the interface zone which allows for interchange of load between the two phases. In case of polymeric fibers, due to hydrophobicity and lack of any chemical bond between fiber and matrix, the weak interface zone limits the ability of the fibers to effectively carry the load that is on the matrix phase. Depending on the fiber's surface asperity, shape, chemical nature, and

`

mechanical bond characteristic of the load transfer between matrix and fiber can be altered so that the final composite can be improved. These modification can be carried out by means of thermal treatment, mechanical surface modifications, or chemical attack, however they require proper optimization. The objective is to determine the mechanical properties of macro-synthetic fibers and develop guidelines for treatment and characterization that allow for potential positive changes due to exposure to ionizing radiation. Fibers are exposed to various levels of radiation and the tensile, interface and performance in a mortar matrix are documented. As a final task, the scale up investigation will be evaluated to address the potential industrialization of the irradiation treatment in order to address the feasibility of the proposed project from a production standpoint.

1.1.1 Irradiation Process:

Certain nuclides are radioactive, that is, they are unstable and seek decay into stable configuration. Protons (+ charged) in the nucleus repel one another because they are positively charged. Neutrons in the nucleus act as a glue to hold nucleus together. However there is a need for balance for number of proton and neutrons.

Figure 1 shows stable nuclides, which have a balance of protons and neutrons. Nuclides to the right of the belt of stability have an excess of proton and seek to reduce the number of protons for example by alpha emission, positron emission, and electron capture. Radioactive atoms are characterized by their decay constant, λ. The decay constant is the probability that an atom will decay. The decay constant is independent of pressure,

`

temperature and chemical form. The decay constant is more commonly expressed as half-life. [5]

$t_{1/2} = \ln(2) / \lambda$

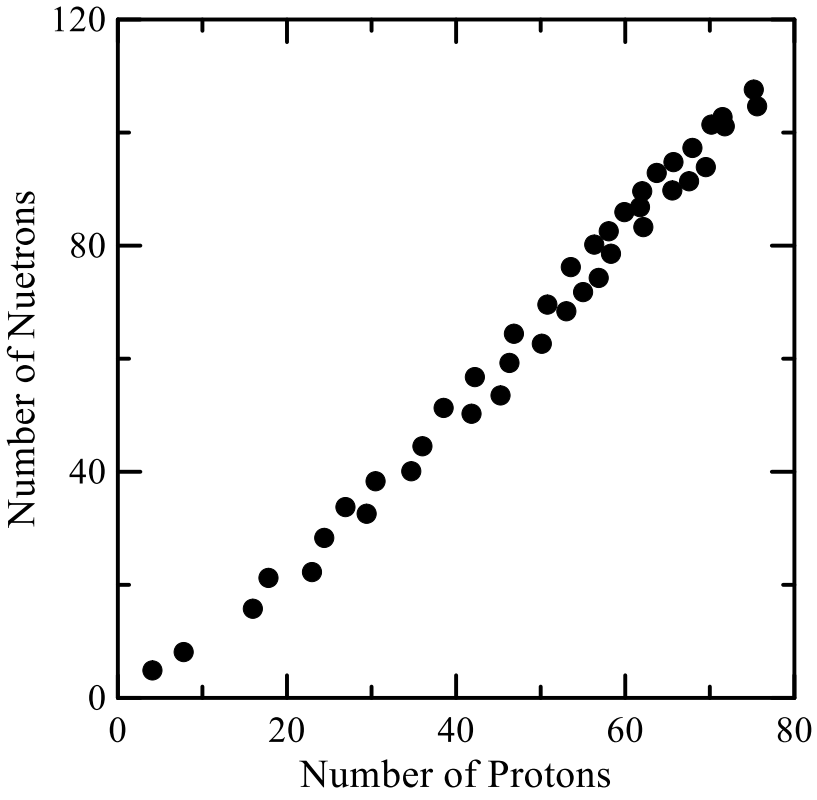

Figure 1: Neutrons vs Protons balance plot. [5]

In other words, nuclei undergo radioactive transformation because constituent in the nucleus are not arrayed in the lowest potential energy state possible, therefore, a rearrangement of nucleus is transformed to an atom of a new element. The transformation

`

of nucleus may involve emission of alpha particle, electromagnetic radiation in form of gamma rays.

Radioactive decay is the process by which an unstable atomic nucleus loses energy by emitting radiation such as alpha rays, beta particle and gamma rays. A material containing such unstable nuclei is considered as radioactive. Gamma rays have energies above 100 keV, and have frequencies above 10 exahertz (or $>10^{19}$ Hz) and wavelengths less than 10 picometers (10^{-11} m).[6]

Gray is the international derived unit (SI) for ionizing radiation dosage. The gray (Gy), which has units of joules per kilogram (J/kg), is the SI unit absorbed dose, and is the amount of radiation required to accumulate 1 joule of energy in 1 kilogram of any kind of matter. Absorption of gamma ray is dependent on thickness of layer, density, and the absorption crosssection of material.

1.1.2 Effect of radiation on fiber morphology and cement composites:

High energy radiation initiates polymerization to join monomer upon polymeric chains. Low energy radiation such as ultraviolet is less penetrating and has been restricted to surface treatment. Major advantages of irradiation are: (a) reaction can be carried out at lower temperature. (b) Monomer can be polymerized free of catalyst contamination. (c) Coating can be applied in monomeric form, eliminating solvent. [7]

Machnowaski [8] studied the effect of gamma radiation on the mechanical properties and surface structure of fabric made up of cotton, flax and silk fiber. The fabric was irradiated with gamma rays (^{60}Co source) and with four different dosage dosages at ambient

`

temperature: 5, 10, 25 and 100 kGy. Mechanical (tensile) test were performed on the fabric samples. The test results showed a clear effect on the breaking force and elongation of the fiber at break. It was observed that the irradiation reduced the strength of the fiber and in particular for high radiation. Among the tested fabric, linen fabric showed a decrease in its strength by 33% for 100 kGy of ionizing radiation in comparison to cotton fabric where the decrease in strength was almost 28 %. One the contrary, irradiation of fiber with lower dosage between 5-25 kGy does not cause a drastic deterioration in the tensile strength and maximum loss reported in this was 14%. The decrease in the strength for high radiation is due to degradation of small individual flax fiber and due to degradation of some non-cellulosic impurities, which bonds this fiber together.

A study was conducted on the effect and modification on polyethylene and Kevlar -49, irradiated to influences between 2×10^{12} to $5\times10^{15}\,\mathrm{cm}^2$ with N^+, Ar^+, Ti^+, Na^+ and He^+ ions . [9]. The irradiated fibers showed softening or melting of fibrillated tendrils with decrease in its tensile strength, when exposed to high energy and dosage of radiation. However, SEM images of Kevlar showed no morphological changes at 20000x magnification.

In addition to polyethylene and Kevlar, a study was conducted on the effect of gamma radiation on mechanical properties of carbon nano tubes and tensile testing was done for a specific gauge length (10 mm) by M. Miao. Average improvement of 27% in tensile strength and improvement of mechanical properties was observed once the fiber was irradiated to a total dosage of 250 kGy. [10]

`

This can give a clear idea of how surface modification of fibers affects fiber matrix bond and the study can be correlated to gamma radiation effect.

Borcia et. al studied the effect of plasma treatment for surface treatment of polymer fiber by using contact angle measurement and adhesion parameters [11]. A comprehensive pullout technique on optimal condition of polyethylene fiber on their interfacial property with cement matrix was reported in a study by Wu [12]. Matrix bond was studied using single fiber pullout test. Polymeric fiber in general has poor interfacial bond strength and poor bonding characteristic, limiting performance with cementitious material. A minor reduction in the tensile strength of the fiber was observed (less than 10%) and the effect was stated as change in surface phenomena rather than change in bulk properties. Second peak or strain hardening effect was observed for the test result. It was suggested that the profound abrasion damage might have given rise to the second peak. A significant increase in the friction bond (2.8 times) and toughness (3.4 times) was observed in the results.

`

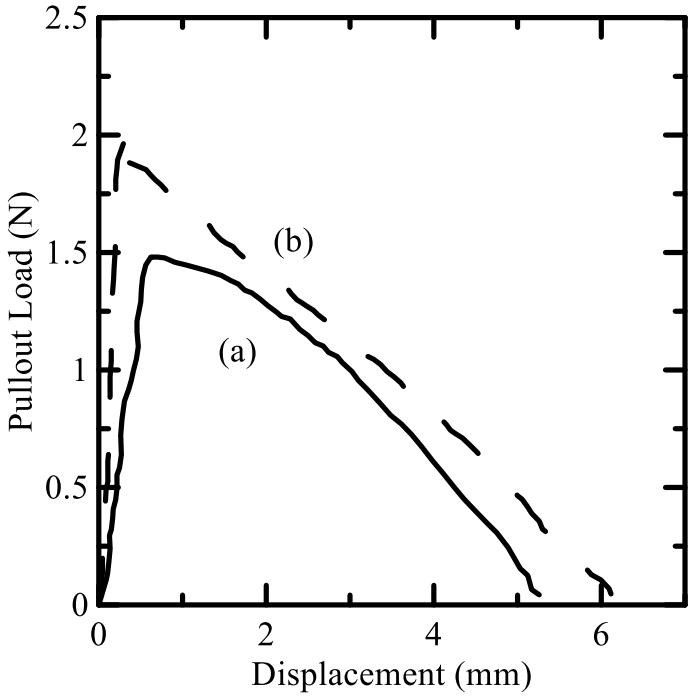

Figure 2: Typical pullout curves of oxygen plasma treated fibers with 100 W, showing chemical bonding (a) treatment time= 1 min (b) treatment time= 5 min. [12]

Treatment of polymer concrete can be done by different procedures, including chemical reaction, heat or radiation. In the case of chemical reaction, a free radical initiator is necessary, such as organic peroxide, it begins cross-linking reaction between the unsaturated resin and a monomer. When using gamma radiation on polymers, three main processes occur: crosslinking and grafting of chains (which involves generation of free radicals). There is insufficient information available on effects of gamma radiation in composites of the type polymer matrix + mineral aggregates + polymeric fibers.

The high-energy ionizing radiation, such as gamma rays (electromagnetic energy) has been used for decades to modify the physical and chemical properties of polymeric materials. This type of radiation promotes ionization and excitation in the irradiated material to produce free radicals that are highly reactive species. Ionization and excitation

`

in the material tend to react with neighboring atoms, eventually causing cross-linking or scission of the polymer chains [13]. Modifications caused by gamma radiation in the physicochemical properties of polymer depend of several parameters as: amount of absorbed energy per unit mass (dose), irradiation conditions including type of gas (air, N_2, etc.), and irradiation temperature. The radiation is the only source of energy which can initiate reactions at any temperature, including room temperature under any pressure, in any phase, whether solid, liquid or gas, without the use of catalysts.

A recently developed method for modifying the mechanical properties is by means of gamma radiation to change the nature of polymeric fibers [14]. This approach was evaluated by microscopy as well as documenting the mechanical properties of irradiated polymeric fibers. Morphological modifications in the irradiated fiber may improve or deteriorate the final product [15]. Irradiated polypropylene fiber (5 kGy) increased tensile strength by 14% in comparison to the non-irradiated fiber. However, at 50 kGy both tensile strength and tensile modulus decreased significantly. Results of this study suggest that reduction of tensile strength and modulus are related with the combinations of two morphological changes: wrinkles and particles on the surface. In general, modification can be controlled by selecting an adequate dose [16]. Effect of gamma radiation in polymer concrete reinforced with luffa fiber was studied by Martínez-Barrera et. al. [17] [18]. Nylon fibers demonstrated an enhancement in the mechanical properties of the concrete due to gamma irradiation [19,20]. In nylon crystalline regions, two phenomena take place: the melting temperature decreases and the heat capacity increases when the gamma radiation is increased. At 10 and 50 kGy levels however, a lowering of the

`

compressive strength was observed. By contrast, 100 kGy “ductile” fibers increased the compressive strength of fiber reinforced concrete. Such mechanical changes are a consequence of morphological changes produced by gamma radiation.

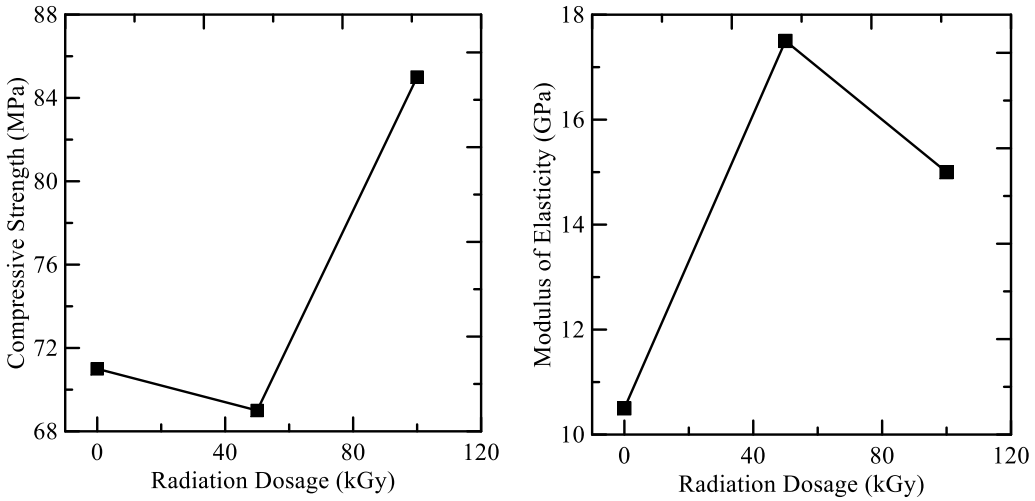

Figure 3: (a) Compressive strength of polymer concrete with 0.3% luffa fiber, irradiated at 50 kGy 100 kGY. (b) Modulus of elasticity of polymer concrete with 0.3% luffa fiber, irradiated at 50 kGy 100 kGy [17]

Both luffa fibers and gamma radiation are already adequate methods for improvements of the mechanical properties of polymer concrete. To obtain an improved polymer concrete, it is recommendable to use 0.3% of concentration of luffa fibers and an irradiation dose of 100 kGy. Luffa fiber was used due to its physiochemal properties and abundance . Mechanical properties like compressive strength gradually decrease as the concentration of luffa fiber increases. For highest fiber concentration and smallest particle size, the compressive strength decreases by 43%, deformation decreases by 9% and the modulus

`

of elasticity decreases by 15%. Nevertheless, when irradiated, the properties of the concrete improve greatly: modulus of elasticity by 40% and compressive strength by 20%. These changes are attributed to cross-linking of polymer chains produced by gamma radiation.

Barrera studied the effect of gamma radiation on the properties of polypropylene fiber reinforced polymer concrete [21]. During early investigations, textile fibers were used as reinforcements of polymer concrete incorporating 1 and 2% by wt. of chopped textile fibers. Results showed compressive strength decreases of 30% and 43% in comparison to the plain unreinforced polymer concrete. Moreover, bending strength behavior showed that failure was less brittle as textile fibers content was increased [22]. There were four variations with the polymer concrete formulations with and without fibers and irradiation. They were listed as 1) non-irradiated (PC taken as control; without fibers or treatment); 2) irradiated; 3) with fiber addition and 4) with fiber addition and irradiated. As the increment of gamma radiation dose increased, the following behavior was observed for the compressive stress: a) two well-defined stages are seen for each fiber concentration. During the first stage the compressive stress or strength values increased according to the gamma radiation dose up to 250 kGy. In the second one for higher dose the compressive strength values decrease. b) The maximum values of compressive strength are achieved at 250 kGy. An explanation for such behavior seems to be related to the radiation effects on the polyester resin, the irradiation causes chain relaxation and cross-linking having a maximum effect at 250 kGy; and for higher doses chain scission (degradation of polymeric chain) begins and in consequence lower compressive stress values are present.

`

Effect of shielding properties of limestone concrete due to gamma ray irradiation and steel fiber addition was also studied. Cylindrical samples of steel fibers reinforced limestone sand concrete of 10 cm diameter and different thickness in cm was placed in front of the gamma ray flux emitted by Cs-137, Na-22 and Co-60 gamma ray sources. The transmission of narrow beam through layer of different material was measured and quantified with respect to photon incident energy [23]. The mass attenuation coefficient μ/ρ which can be defined as:

$$\mu/\rho = t^{-1}\ln(I_O/I_t) \quad (1)$$

Where I_O the intensity of the incident photon beam is measured and I_t is the intensity of the transmitted beam. According to bad geometry case there will be more gamma flux encountered by the detector. The result of the calculation will be larger by a certain factor as indicated by following equation:

$$I = B(t, E_\gamma) I_O e^{-\mu x} \quad (2)$$

Where $B(t, E_\gamma)$ is the buildup factor and E_γ is the gamma ray energy. Magnitude of buildup factor depends on the material used and on γ ray energy. From their experimental results of the gamma ray for fiber concrete under investigation, it was concluded that the total mass attenuation coefficient is increased with the increasing fiber content up to 3% steel fiber weight. Addition of 3% wt. steel fiber to their concrete improves the total mass attenuation coefficient by a factor of 1.52. The buildup factor increases with the

`

increasing concrete thickness and with the increasing concrete density. The maximum value of the buildup factor found at 3% wt. of steel fiber addition to concrete.

Barrera et. al also studied the effect of polyester fiber and gamma irradiation on mechanical properties of polymer concrete containing $CaCO_3$ and silica sand [24]. In this study nylon surface was modified by gamma radiation dosages. Tensile strength of the irradiated fibers was determined and then the fibers mixed at 1.5%, 2.0%, and 2.5% in volume with Portland cement, gravel, sand, and water. The highest values of the compressive strength of fiber reinforced concrete (FRC) are seen for fibers at 50 kGy and 2.0% in volume of fiber; the strength is 122.2 MPa, as compared to 35 MPa for simple concrete without fibers.

We advance a mechanism by which the fiber structure can be affected by gamma irradiation resulting in the compressive strength improvement of the concrete. The tensile tests on the fibers were a carried out according to the ASTM D638 standard. Average values of the tensile stress at yield points of the fibers as a function of the irradiation at 50 kGy dose the tensile stress at yield amounts to 701.6 MPa, a 144% above the value for non-irradiated fibers.

`

1.2 Irradiation Instrument:

A Gamma Cell 220 self-shielded irradiator with the Co-60 source was used to irradiate the fibers in this study. Cobalt 60 or ^{60}Co is a synthetic radioactive isotope of cobalt. It is produced artificially in nuclear reactors. ^{60}Co is extensively used because of its long half life of 5.27 years.[25] Dosage rate for the fiber was about 3.5 Gy/min (350 rad/min).

Figure 4: Gamma Cell 220 Self-Shielded irradiator with Co-60.

`

1.3 Structure of the Thesis

The motivation of this study is to evaluate the effect of irradiation on the mechanical properties and bonding characteristics as well as the performance of polymeric fibers for use in concrete. A series of experiments were conducted by exposing polypropylene fibers obtained from Forta corporation to different levels of gamma radiations. Samples were subjected to three doses of irrradiation. The irradiated samples were then subjected to three levels of testing that include fiber tension test, pullout test , and flexural strength and post peak residual strength from mortar blends. Properties of individual fibers, interface characteristics and behavior when mixed in a mortar blend were mesured and presented in various sections of this report. Fiber reinforced concrete (FRC) beams using Forta fiber were prepared and tested in the Computational and Experimental Mechanics Laboratory in Arizona State University. All the specimens were cured under identical conditions in a curing room maintained in a controlled environment of 73^{o} F and 100 % RH until the day of testing. Fiber pullout as well as four-point bending tests were performed on the beams cast after 28 days of normal curing. Synthetic fiber include polypropylene, polyethylene, and nylon.

Tensile test on three gamma irradiation treatment at a range of irradiation dosages (5, 35, and 70 kGy) and for a specific rate was carried out for 70 samples. Tensile test is used in determination of effective properties of fiber and to characterize the fiber in accordance to their radiation energy. Fiber essentially carry load in a system of composite and its properties can be used in micromechanics modeling.

`

Pullout test was done on irradiated and non-irradiated fiber, for a specific displacement rate (0.02 mm/min) for 50 samples. Single fiber pullout test is employed experimentally to model failure of fiber reinforced concrete. Complete description of experimental events is presented and described in a closed loop model, shear stress of the bond is calculated.

Flexural strength as a measure to estimate the tensile strength of concrete was carried out for 18 samples. Flexural test is done to estimate various effective strength based parameters like toughness (T (L/150)) and post peak equivalent stresses (f150) response. Flexural test is used to estimate the post peak response of the specimen. Flexural test was carried out for irradiated and non-irradiated fibers. Flexural strength is highly sensitive to volume fraction of fiber. A constant volume fraction (0.5%) is used to prepare mix for all the batches.

`

2 FIBER TENSILE TEST

2.1 Introduction

Polypropylene Fiber blend manufactured by Forta Corporation, Grove City, PA, USA, consists of heavy duty copolymer monofilaments. These fibers are used for improved post crack benefits in concrete structures and fibrillated polypropylene fiber for crack control. Polypropylene fibers are typically used in long lengths (such as $2-1/4$ inch) and in high dosages (3-30 lbs per cubic yard) to affect the higher replacement level of reinforcing steel than synthetic fiber. Forta fiber is supplied in a bundle, each consisting of 15 to 17 yarns. It was assumed that an average of 16 yarns were used in a single bundle of Forta Fiber.

2.1.1 Diametric Measurement:

Due to fibrillated nature of the (Forta) polypropelene fiber, calculation of diameter of the single yarn of fibers is not possible with a normal Vernier caliper measurement. As the shape of the fiber yarn changes due to fibrillated nature of the fiber and as it does not have a perfect circular cross section, an area measuring approach was used to get an approximate diameter of a single yarn of fiber. Diameter of the fiber is an important point of concern when it comes to stress strain response and pullout simulations. Two methods were used for the calculation of area:

1. Mass and density approach, and
2. SEM test and image analysis approach.

`

2.1.1.1 Mass and density approach.

In this method 100 mm of single yards are weighted and then with the help the specific gravity provided by the manufacturer (Forta) area or the diameter of the yarn is back calculated. The specific gravity of the polypropylene fiber is 0.9. Table 1 explain the specimen weight and diametric measuring for the single yarn. This gives an approximate estimation of what the actual diameter could be. The variation in the measurements could be due to varied fibrillated filament in a single yarn of fiber. So the average diameter for a single yarn is 0.53 mm with a standard deviation of 0.03. Similarly for two yarns the estimated diameter is 0.74 mm with a standard deviation of 0.05.

Table 1: Weight approach diametric calculation

Length (L) (mm)	Weight (W) (mg)	Area(A) (mm^2)	Diameter D (mm)
100	19.8	0.22	0.53
100	17.5	0.19	0.50
100	23.2	0.26	0.57
100	18.1	0.20	0.51
Average			0.53
Std. dev			0.03

`

2.1.1.2 Scanning Electron image (SEM) analysis:

For more detail study of the cross section of fiber, SEM image analysis was done for 3 sample. Image J software was used to calculate the area of fiber from the varied fiber cross section. Multiple measurements were taken for the images obtained by SEM. The results of the image analysis is tabulated in Table 2 and SEM images of the cross section are shown in Figure 5. From the obtained area measurement after the image analysis is done approximate diameter of the fiber is estimated. The average diameter of the sample was calculated as 0.52 mm with a standard deviation of 0.02 mm and difference could be due to fibrillated nature of the fiber along with some measurement error. Similarly for two yarns the estimated diameter is 0.73 mm with a standard deviation of 0.02 mm.

`

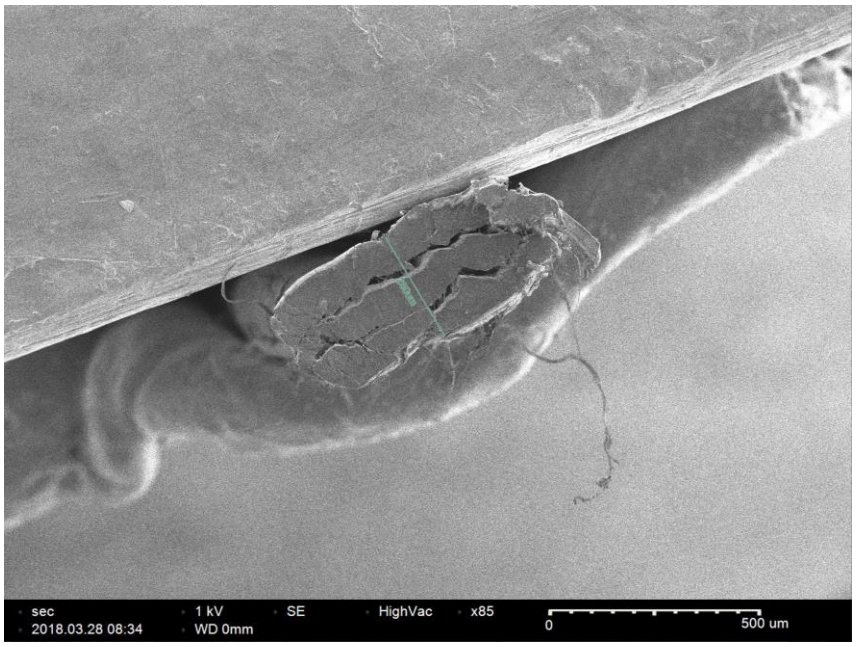
sec
2018.03.28 08:34
1 kV
WD 0mm
SE
HighVac
x85
0
500 um

(a)

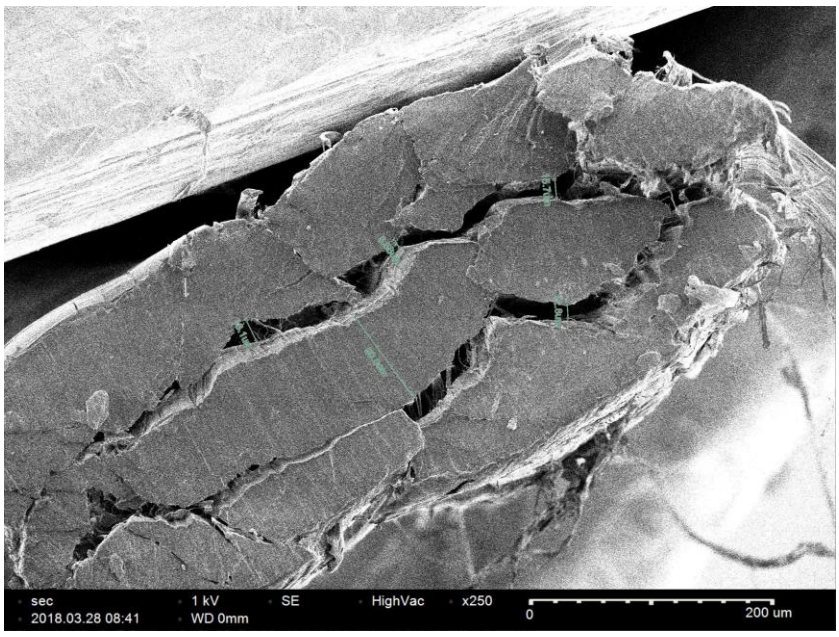
sec
2018.03.28 08:41
1 kV
WD 0mm
SE
HighVac
x250
0
200 um

(b)

`

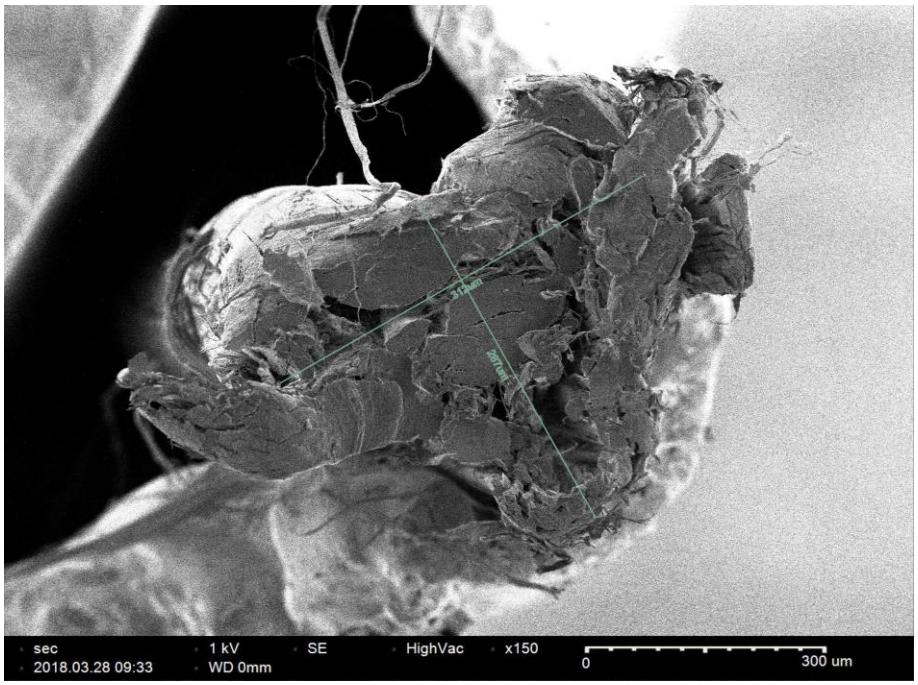

(c)

Figure 5: SEM image cross section of samples. (a) Sample 1, scale: 500 μm, magnification: 85x. (b) Sample 1, scale: 200 μm, magnification: 250x. (c) Sample 2, scale: 300 μm, magnification: 150x.

`

Table 2: SEM image image analysis results.

Sample ID	Trail	Area (mm^2)	D (mm)
1	1	0.239	0.552
	2	0.217	0.526
	3	0.223	0.533
2	1	0.198	0.502
	2	0.189	0.491
	3	0.186	0.487
Average		0.209	0.515
Std. dev		0.021	0.026

2.2 Experimental Program

Fibers were tested under a uniaxial state of tension. The variables in these experiments were the level of irradiation used, effect of different fiber length, and the effect of rates of loading.

The tension test was performed and documented in 3 phases:

1. Using the same gauge length but with different displacement rate.
2. Using the same displacement rate for different gauge lengths.
3. Effect of duration of irradiated samples for different radiation intensities keeping a specific gauge length and displacement rate.

Direct Tension test was performed on Fibers in the structural and material testing laboratory in Arizona State University. Tests were conducted in a MTS 810 system servo hydraulic system. A section of the roving was obtained from the spool, the twisted roving was spilt to 15 to 17 number of individual yarns as a standard testing unit.

`

Separation of the yarn beyond this level exposed the film and therefore definition of fiber was not possible beyond this level. A picture of the yarn section is shown in Figure 7.

A universal joint was connected to the testing frame to allow rotation of the grip and to remove any potential twisting or bending. The universal joint also helps in the alignment of yarn during the test. Since the microfiber has a smooth surface finish, samples encountered significant slip on the application of tensile load. To reduce the slippage, arrest the slip and capture true stress strain response of the specimen, frictional grips as shown in the Figure 6 were used. The fiber was fed and wrapped around the mandrel on the upper grip. After the cross head was moved to the gage length position, the fiber was aligned and wrapped along the bottom grip mandrel. The fiber was then secured in the mandrel using frictional wedge screws. The extensometer was mounted using rubber bands as shown in Figure 6. Both the displacement from the extensometer as well as the stroke response of the equipment were measured and reported. Tests were conducted using displacement control test at three different rates of 0.1 in. /min, 0.5 in. /min and 2.5 in/min. Figure 6 shows the specimen with the grip with the extensometer attached. Note that the gage length of the extensometer was used in the calculation of the fiber stiffness to avoid the spurious deformations that take place due to fiber slip gauge at the support.

`

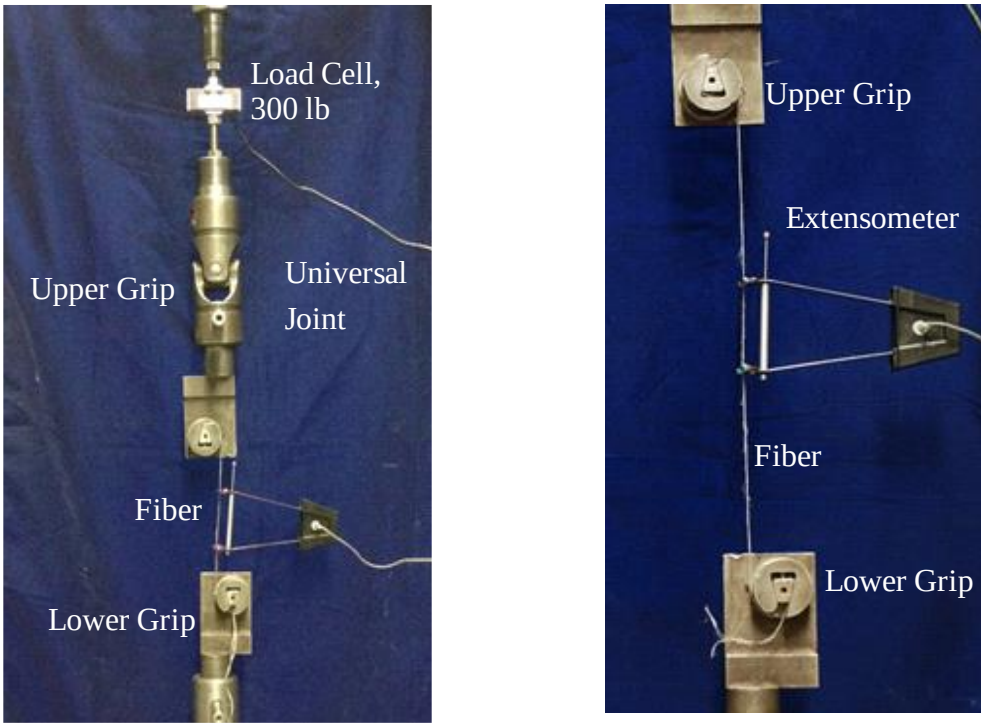

Figure 6: (a) Experimental setup. (b) Alignment of extensometer with Fiber.

To maintain the reproducibility of sample extraction, form a bundle, an average number of 2 yarns was used for the Fiber Tension Test. This results in a homogeneous sample collection and used in the calculation of effective fiber diameter using results for a single bundle of fiber.

`

Figure 7: E-scope image of Forta Fiber.

2.3 Test Results

Two yarns were tested together on an MTS 810 test frame under displacement control. The specimen was not perfectly vertical prior to the test. This is due to the free tilt of the fixture in the presence of universal joint. However, as test starts, and load increases the specimen aligns perfectly. The sample was loaded to failure , At the peak load signs of crazing were evident within the loading period, The strength was reached after significant plastic deformation. Average values of engineering strain were in the range of 25 to 30 %.

`

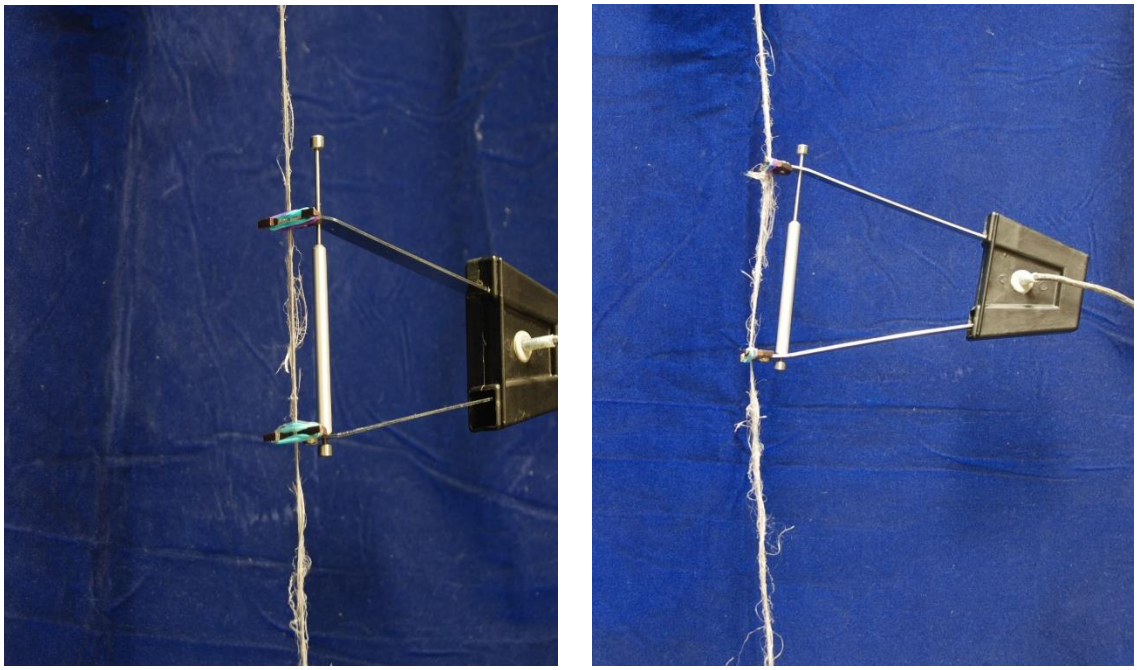

Figure 8 :(a) Fiber under the load prior to the ultimate strength with signs of crazing, (b) Fiber failure after the test.

The load-displacement responses from the actuator and the extensometer were processed and stress-strain responses were deduced. Figure 9 shows a typical tensile test result. The different ranges of the response are identified in the Figure 10 and Figure 11.

Initial loading, crimp removal elastic range, plastic ozone, ultimate strength and the post peak range are shown. The stress-strain responses measured from these tests are summarized in the appendix. The strain measures reported here are recorded from the 2-inch extensometer and stress is recorded from the 300 lb. Instron load cell. The data recorded from the actuator are in accordance with the extensometer readings.

`

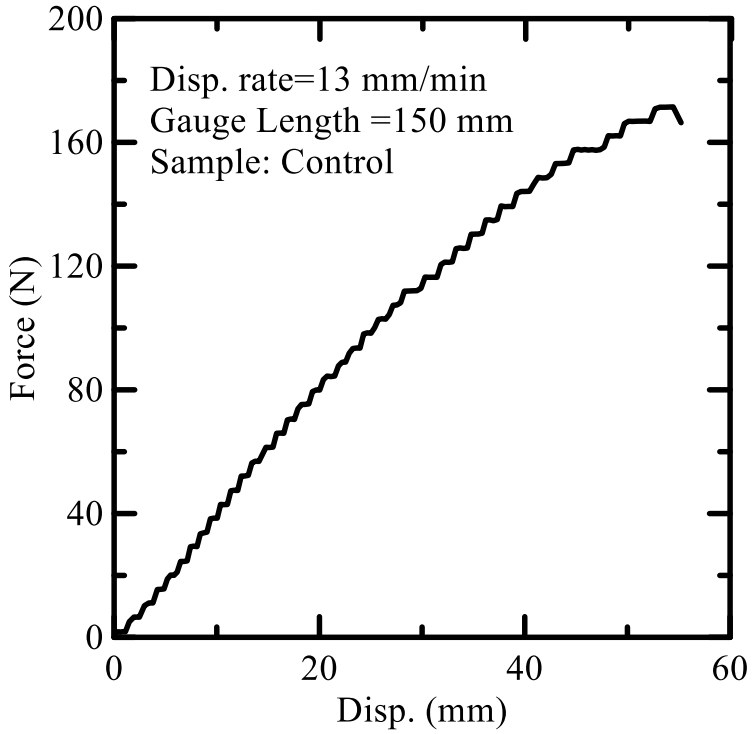

Figure 9: Single Fiber tensile result.

`

Table 3: Summary of uniaxial fiber tension test samples.

No.	Type	Gage Length	Stroke Displacement	# Replicates	Total Samples tested	Test Date
		mm(in)	mm/min (in/min)			
1	Non-irradiated	150 (6)	2.54(0.1)	5	7	07/10/17
2	Non-irradiated	150 (6)	12.7(0.5)	5	7	07/28/17
3	Non-irradiated	150 (6)	63.5(2.5)	5	7	07/28/17
4	Non-irradiated	200(8)	12.7 (0.5)	7	8	07/13/17
5	Non-irradiated	300 (12)	12.7 (0.5)	8	9	07/13/17
6	Irradiated (5 kGy)	150 (6)	12.7 (0.5)	4	8	11/08/17
7	Irradiated (35 kGy)	150 (6)	12.7 (0.5)	6	8	07/28/17
8	Irradiated (70 kGy)	150 (6)	12.7 (0.5)	6	8	10/13/17

`

Table 4: Fiber Tension Test results at different stroke rates.

Gauge Length mm (inches)	Stroke Rate mm/min (in/min)	Sample	Max Force (N)	Tensile Strength (MPa)	Strain (%)	Stiffness (kN/m)	Toughness (kN-m)
152.4(6)	63.5 (2.5)	T1	161	374.5	26	0.74	1.25
		T2	191	444.3	23	1.52	2.14
		T3	187	435.0	25	2.35	1.26
		T4	188.5	438.5	25	1.66	1.26
		Average	181.9	423.1	24.8	1.6	1.5
		Std.	14	32.60	1.25	0.6	0.4
	12.7 (0.5)	T1	166	386.2	23	1.00	0.84
		T2	167	388.5	22	0.86	0.81
		T3	168	390.8	23	0.75	0.84
		T4	150.6	350.3	27	0.68	0.92
		Average	162.9	378.95	23.8	0.8	0.9
		Std.	8.2	19.2	2.2	0.13	0.04
	2.54 (0.1)	T1	165	383.8	36	0.51	1.00
		T2	150	348.9	34	0.46	1.35
		T3	144	335.0	27	0.46	0.80
		Average	153	355.9	32.3	0.5	1.1
		Std.	10.8	25.1	4.7	0.02	0.27
Average			167.1	388.7	26.4	0.7	1.13
Std. Dev			16	37.3	4.5	0.18	0.39

`

Table 4 results of fiber properties as a function of displacement rates are shown. It is observed that the average tensile strength of the fiber increases from 388.7 MPa to 423 MPa as the displacement rate increases from 2.54 mm/min to 63.5 mm/min.. This may be attributed to the viscoelastic property of the fiber, average stiffness increased from 0.7 to 1.6 kN/m as the loading rate increased from 2.5 mm/min to higher rates of 63.5 mm/min. Conversely, the average strain value decreases from 32% to 24% for higher rate (63.5 mm/min) compared to lower rate (2.5 mm/min). Average toughness increases from 1.1 kN-m to 1.5 kN-m for the high rate (63.5 mm/min) and high tensile strength at high rate is one of the important factor for the increase. At lower rate of 2.5 mm/min, the average tensile strength of the sample was 1.1 kN-m. The effect of loading rate is clearly apparent in Figure 10. These data can be used in the simulation and modeling of the dynamic response and high-speed performance of the FRC with polymeric fibers.

`

Table 5: Fiber Tension Test results at different gauge length

Gauge Length mm (inches)	Stroke Rate (mm/min) (in/min)	Sample	Max Force (N)	Tensile Strength (MPa)	Strain (%)	Stiffness (kN/m)	Toughness (kN-m)
150 (6)	12.7 (0.5)	T1	166	386.2	23	1.00	0.84
		T2	167	388.5	22	0.86	0.81
		T3	168	390.8	23	0.75	0.84
		T4	150.6	350.3	27	0.68	0.92
		Average	162.9	379.0	23.8	0.8	0.9
		Std.	8.2	16.6	2.2	0.13	0.04
200 (8)		T1	159	369.9	24	0.56	0.83
		T2	155	360.6	27	0.54	1.16
		T3	152	353.6	25	0.56	0.68
		T4	156	362.9	26	0.60	0.67
		Average	155	361.8	25.3	0.6	0.9
		Std.	3.5	5.8	1.5	0.01	0.23
300 (12)		T1	171	397.8	24	0.53	0.6
		T2	155	360.6	23	0.51	0.94
		T3	156	362.9	24	0.51	0.95
		T4	153	355.9	25	0.49	1.07
		Average	160	369.3	23.7	0.5	0.8
		Std.	8.9	16.6	0.5	0.01	.02
Average			159.1	370.0	24.4	0.63	0.86
Std. Dev			7	16.4	1.62	0.161	0.164

`

Table 5 shows results of fiber properties as a function of gauge length. It is observed that the change in the average tensile strength was minimal, when tested as a function of length. The range varied from 379 MPa to 369 MPa as the gauge length is varied from 150 mm to 300 mm. On the same grounds, very small change in the strain and toughness values was obtained, when varied as a function of length. The range for the strain was between 23 to 25% and that for the toughness was 0.85 to 0.9 kN-m. However, the stiffness of the sample decreased as the gauge length increased. Stiffness decreased from 0.8 kN/m to 0.5 kN/m as the gauge length increased from 150 mm to 300 mm. The effect of gauge length is clearly apparent in Figure 11.

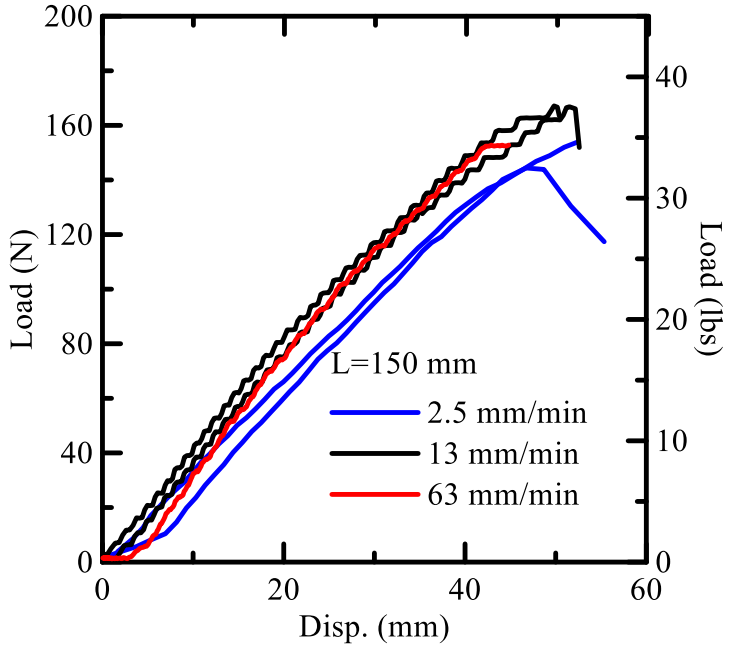
Load (N)
Load (lbs)
Disp. (mm)
L=150 mm
2.5 mm/min
13 mm/min
63 mm/min

(a)

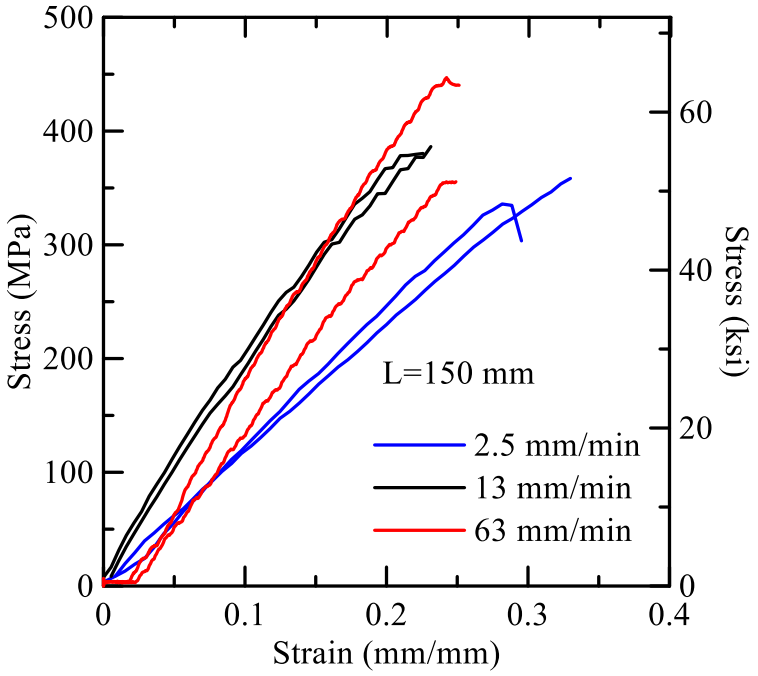
Stress (MPa)
Stress (ksi)
Strain (mm/mm)
L=150 mm
2.5 mm/min
13 mm/min
63 mm/min

(b)

`

Figure 10: Different rates (0.1, 0.5, 2.5 inch/min) response for 6 inch gauge length sample. (a) Force vs Displacement response. (b) Stress vs Strain response.

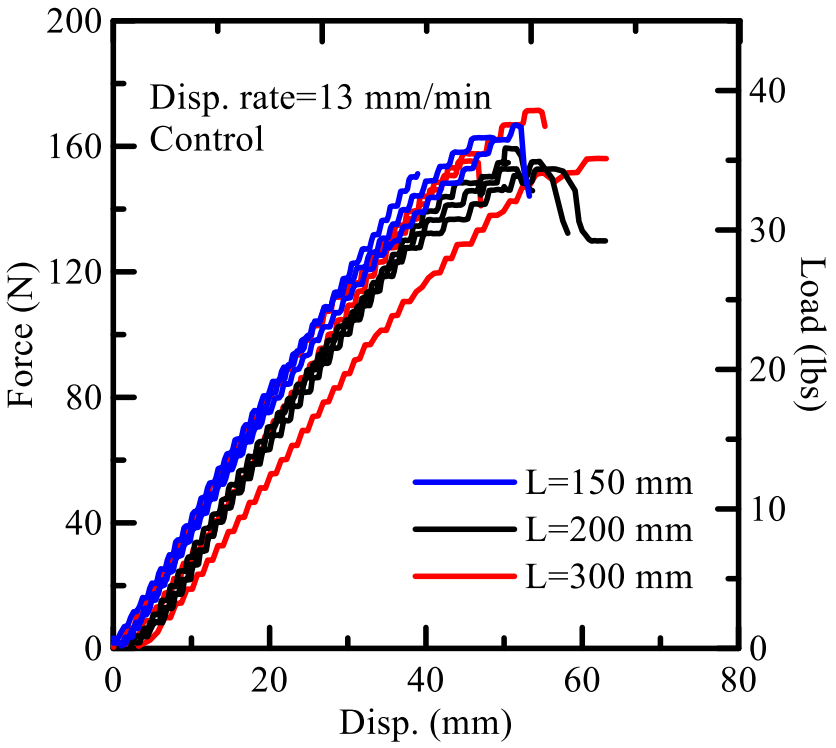

(a)

`

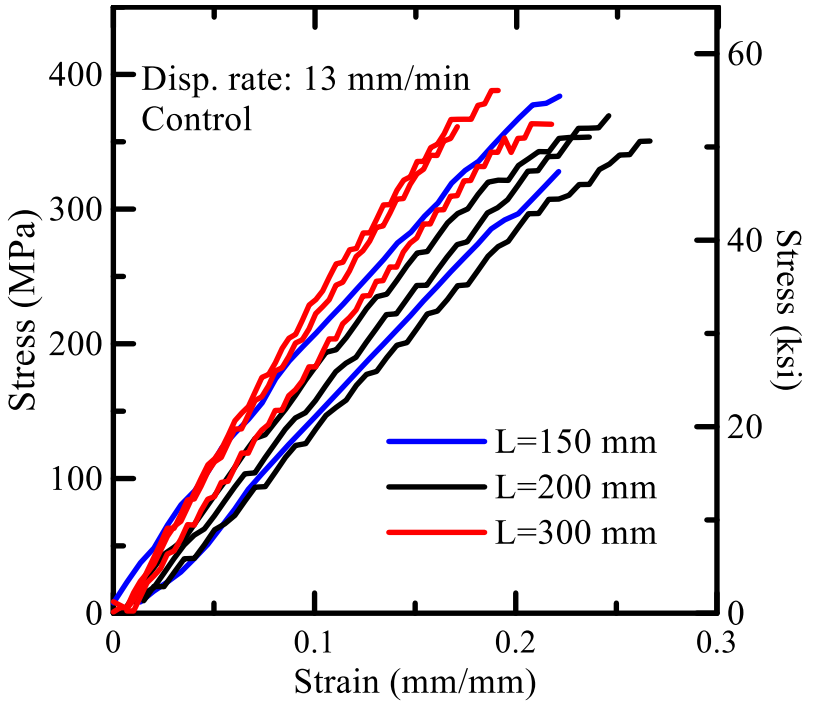

(b)

Figure 11: Different gauge length (6”, 8”, and 12”) response for a constant displacement rate (0.5 in/min). (a) Fore vs Displacement response. (b) Stress vs Strain response.

Table 4 shows the results of fiber properties as a function of different irradiation levels. It is observed that the average tensile strength of the fiber decreased as the radiation level or intensity is increased. Average tensile strength decreased from 413 MPa to 42.5 MPa as the intensity is increased from 5 kGy to 70 kGy. On the same grounds, strain decreased from 24 % to 4% as the irradiation intensity is increased from 5 kGy to 70 kGy. Average stiffness increased from 0.8 kN/m to 0.9 kN/m for 5 kGy sample as compared to the control sample. But for 35 kGy stiffness decreased to 0.42 kN/m. Negligible stiffness was observed for 70 kGy sample as it can be seen from Figure 12 (c), also on the cost of very

`

high decrease in strength. Practically, the only sample where the average stiffness increased in comparison to control sample was 5 kGy sample, without sacrificing the strength parameter.

Table 6: Effect of different irradiation levels on the tensile properties of samples. Disp. Rate: 0.5 in. /min, Gauge length: 6 inches.

Radiation Dose	Sample	Max Force (N)	Tensile Strength (MPa)	Strain (%)	Stiffness (kN/m)	Toughness (kN-m)
5 kGy	T1	167.3	389.2	26	0.78	0.37
	T2	167.1	388.7	23	0.98	0.37
	T3	170.4	396.4	22	0.87	0.34
	T4	205.5	478.1	26	0.94	0.46
Average		177.6	413.1	24.3	0.89	0.39
Std. Dev		18.7	43.5	2.08	0.08	0.05
35 kGy	T1	98	228.0	16	0.72	0.42
	T2	91	211.7	15	0.56	0.42
	T3	104	241.9	15	0.67	0.64
	T4	90	209.4	14	0.7	0.37
	T5	82	190.8	16	0.65	0.27
	T6	97	225.7	15	0.79	0.44
Average		93.7	217.9	15.1	0.68	0.42
Std. Dev		7.7	17.8	0.745	0.08	0.12
70 kGy	T1	17.2	40.0	3.1	Negligible	0.01
	T2	13.2	30.7	3.3		0.012
	T3	21	48.9	3.5		0.027
	T4	21.7	50.5	4		0.014
Average		18.8	42.5	3.4		0.016
Std. Dev		6	9.1	0.4		0.008

`

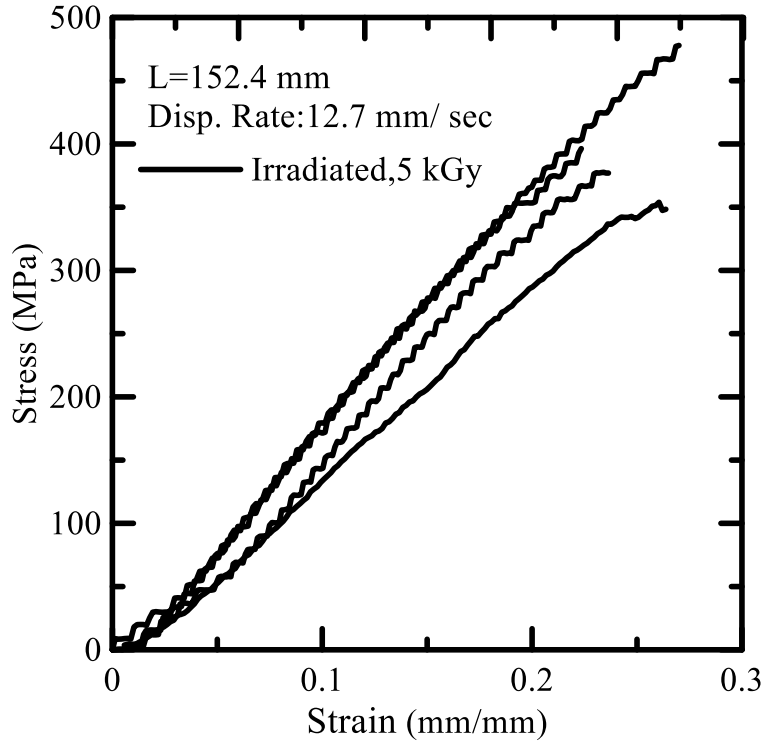
L=152.4 mm
Disp. Rate:12.7 mm/ sec
Irradiated,5 kGy
Stress (MPa)
Strain (mm/mm)
0
100
200
300
400
500
0
0.1
0.2
0.3

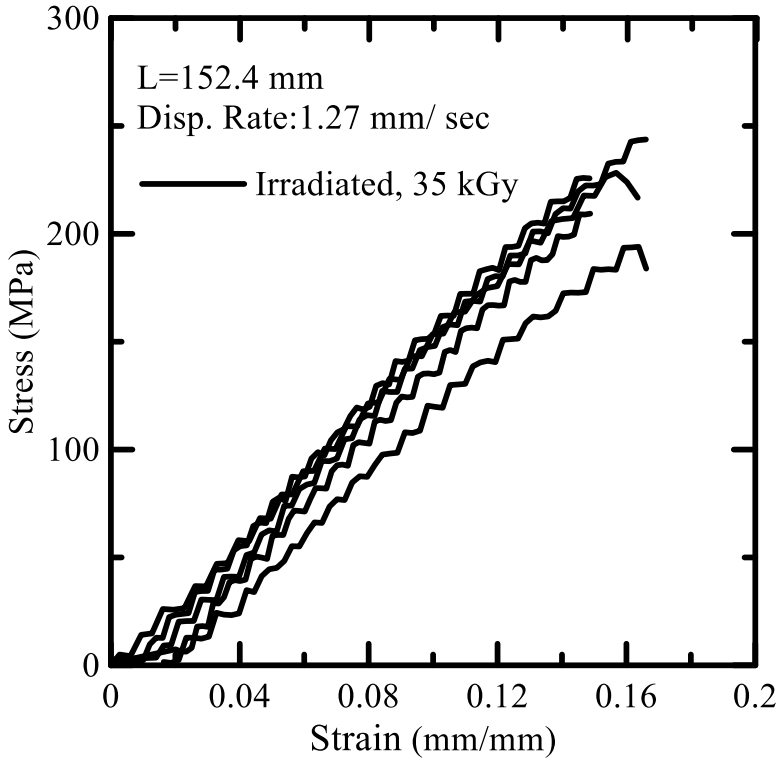
L=152.4 mm
Disp. Rate:1.27 mm/ sec
Irradiated, 35 kGy
Stress (MPa)
Strain (mm/mm)
0
100
200
300
0
0.04
0.08
0.12
0.16
0.2

`

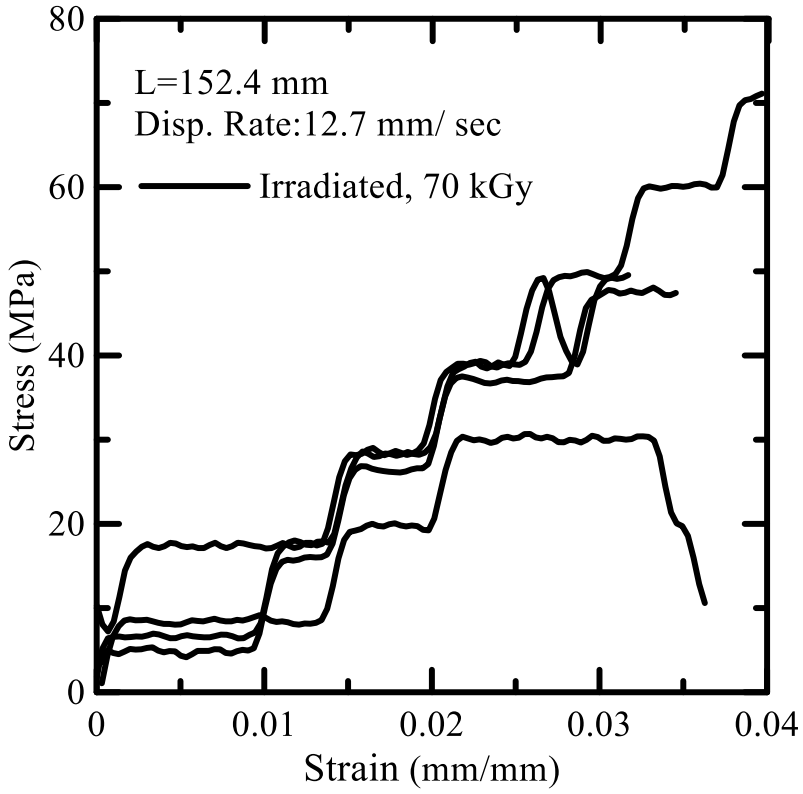

Figure 12: Irradiated Sample results. (a) 5 kGy sample. (b) 35 kGy sample (c) 70 kGy sample.

`

2.3.1 Microstructure examination using SEM (Scanning Electron Microscope)

Figure 13: SEM Test Machine.

Figure 13 shows XL30 ESEM-FEG instrument offering high resolution electron imaging at pressure as high as 10 Torr and sample temperatures as high as 1000^{o} C. The resolution of the SEM is 3 nm. The XL30 ESEM-FEG employs the stable, high brightness Schottky Field Emission Source for outstanding observation performance of potentially problematic samples for conventional high vacuum SEMs.Typical morphological characterization requires that the fiber be vacuum coated with carbon in a vacuum pump and analyzed by scanning electron microscope (SEM), which provides good image distribution of the controlled sample. Figure 14 shows a smooth fibrillated surface of a single fiber filament at different magnification obtained from SEM test.

`

Figure 15 represents the surface characterization at fiber when radiated with 5 kGy of energy. Disturbance on the surface of the fiber at a very low magnification of 65X can be observed in Figure 15 (a). Even at higher magnification we can only observe the surface of the fibrillated filament being affected by the radiation and no kind of degradation was observed for this radiation energy.

Figure 16 represents the surface characterization at fiber when radiated with 35 kGy of dose. It can be observed from the SEM images of the 35 kGy fiber, very little degradation of the fiber at lower magnification of 65 X is observed. However, as the magnification is increased to 1000 X and 2500 X we can clearly observe the degradation on the surface of the fiber due to radiation.

Figure 17 represents the surface characterization at fiber when radiated with 70 kGy of dose. It can be observed that even at a very low magnification a clear degradation of the fiber can be observed. Micro fiber filaments being damaged by the radiation energy, lowering the tensile strength.

`

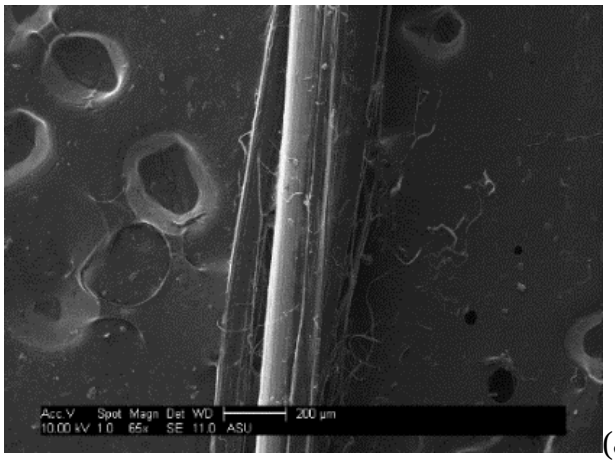

(a)

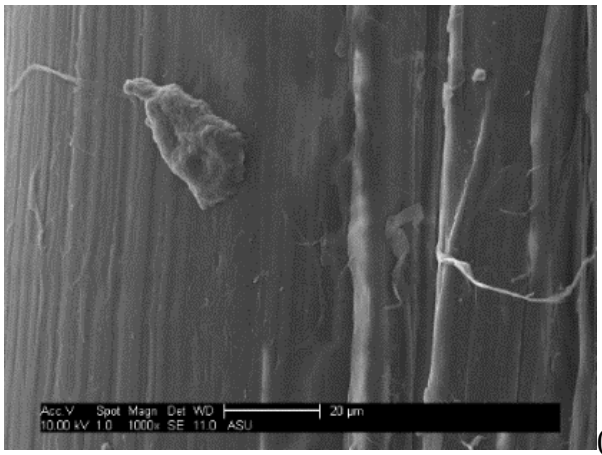

(b)

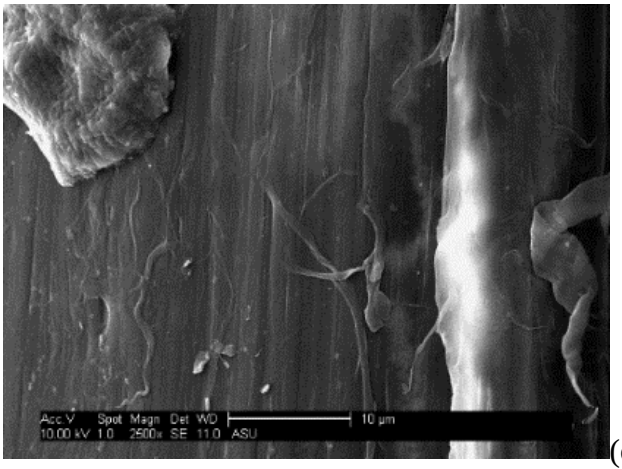

(c)

Figure 14: SEM images of Control Sample at various magnifications, (a) 65X (b) 1000X,

(c) 2500X

`

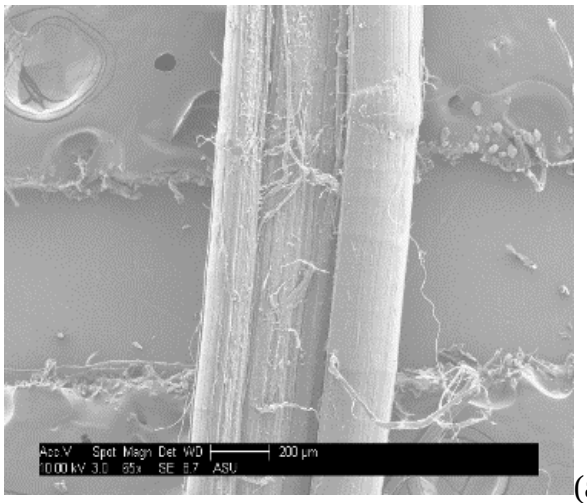

(a)

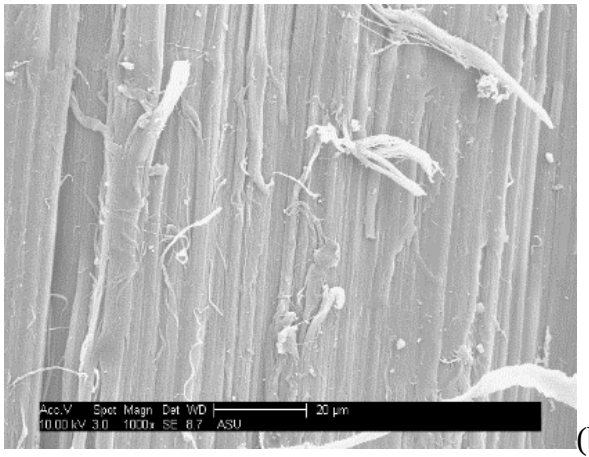

(b)

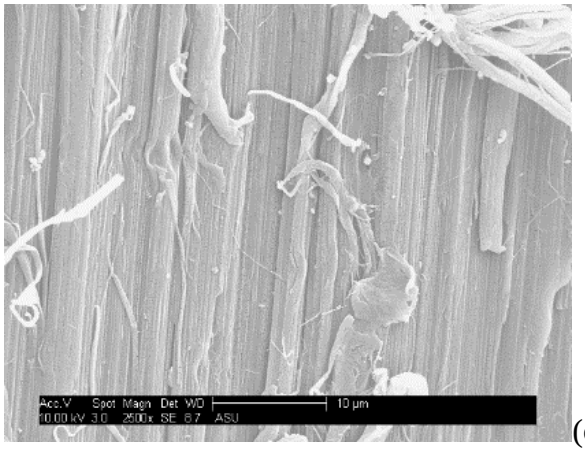

(c)

Figure 15: SEM images of 5 kGy Irradiated Sample at various magnifications, (a) 65X (b) 1000X, (c) 2500X

`

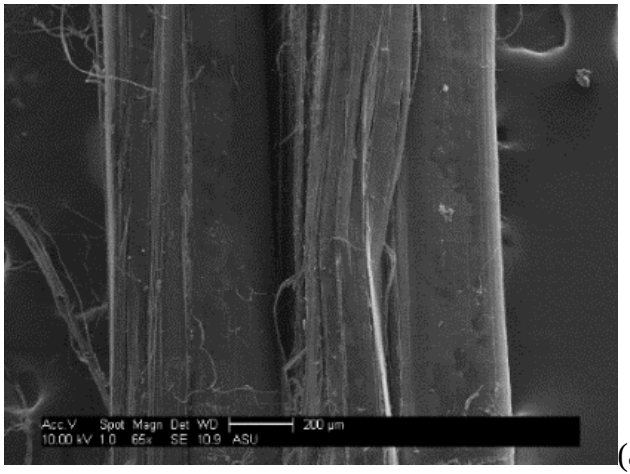

(a)

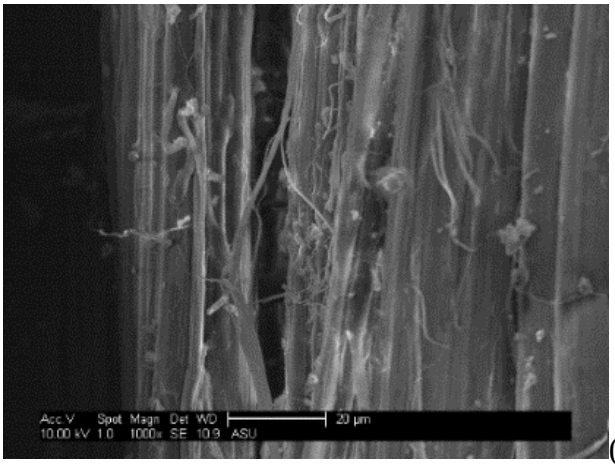

(b)

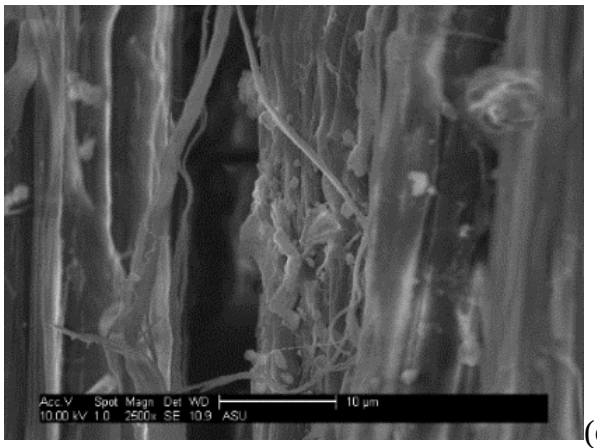

(c)

Figure 16: SEM images of 35 kGy Irradiated Sample at various magnifications, (a) 65X (b) 1000X, (c) 2500X

`

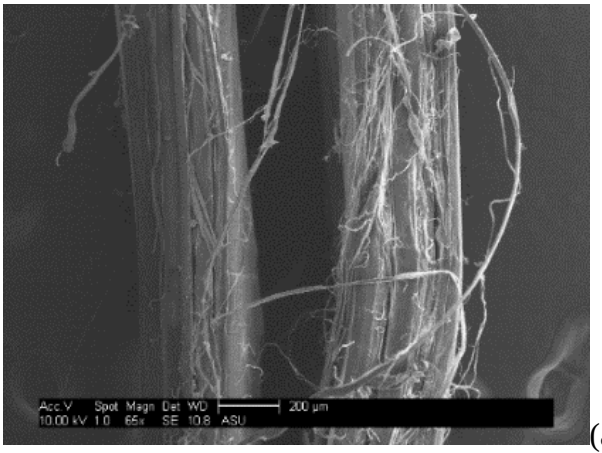

(a)

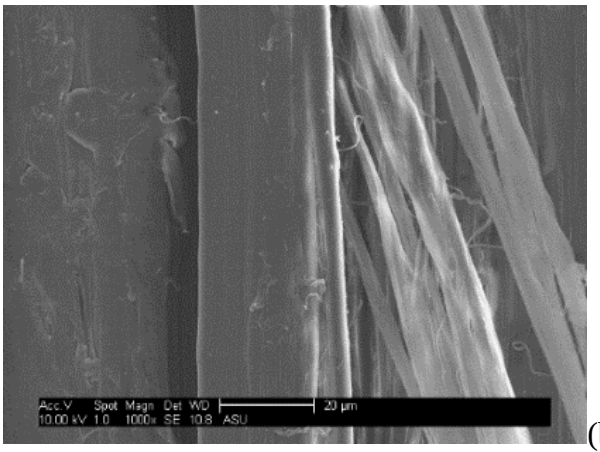

(b)

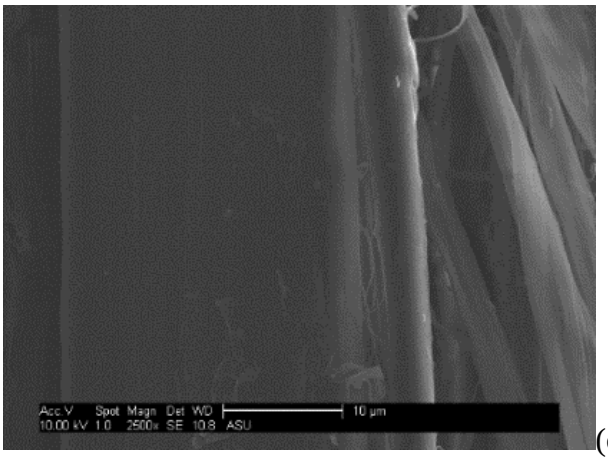

(c)

Figure 17: SEM images of 70 kGy Irradiated Sample at various magnifications, (a) 65X (b) 1000X, (c) 2500X

`

2.3.2 Effect of Irradiation level on the fiber Performance

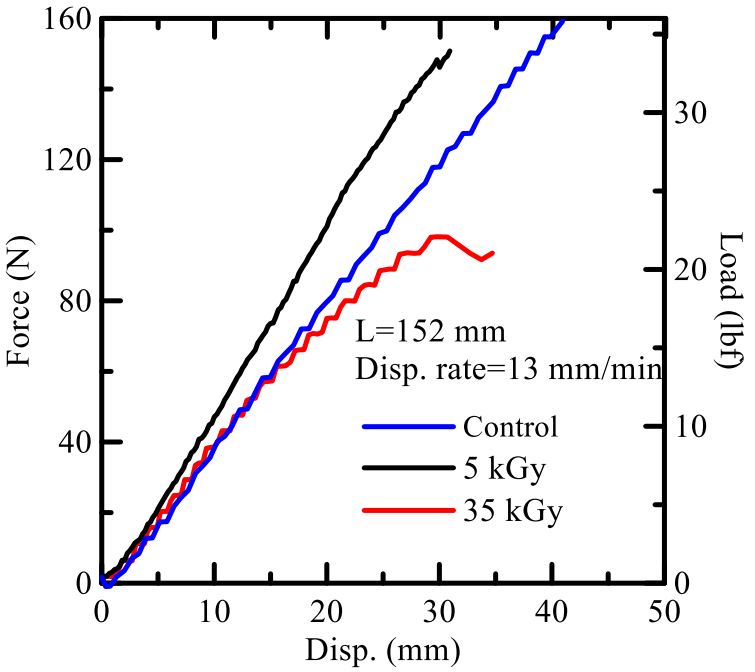

(a)

`

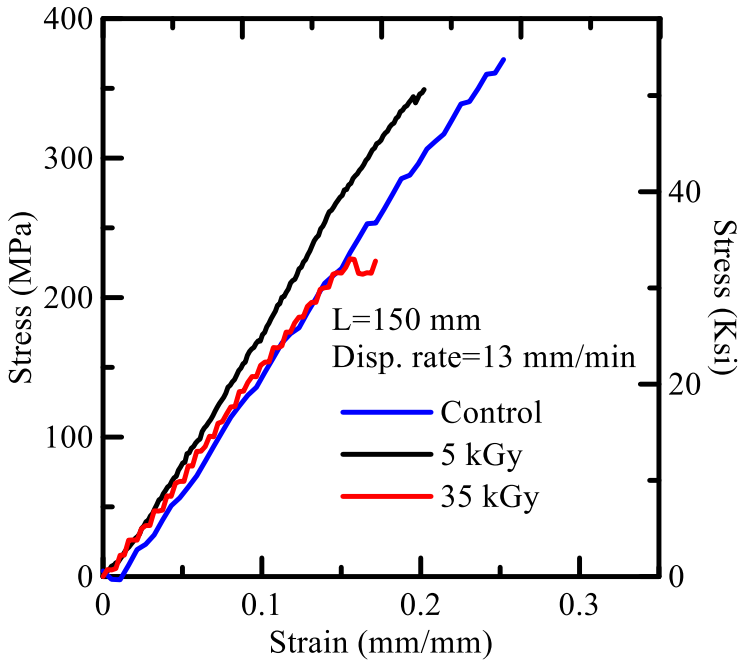

(b)

Figure 18: Radiation energy comparison for a specific gauge length (6") & disp. rate (0.5 in/min). (a) Force vs Displacement. (b) Stress vs Strain.

After carrying out fiber tensile tests with multiple radiation energy for a specific gauge length and rate in quasistatic loading condition flexibity and strength parameter of the polypropelene fiber was assesed. Three differences in the results are discussed in terms of tensile strength, strain capacity and stiffness. The strength data was observed to decrease with the increase in the intensity of radiation. When irradiated with 5 kGy of dose the average tensile strength went from 379 MPa (Control) to 413 MPa, average improvement of 9% in the tensile strength was reported for this radiation dose. Also an increase of 11% in the stiffness values was observed for 5 kGy of radiation, where the stiffness values went up from 0.8 kN/m to 0.9 kN/m. Conversly, when radiated with a comparatively high

`

radiation dosage of 35 kGy and 70 kGy, the tensile strength went down from 379 MPa (Control) to 217 MPa, which is around 38 % decrease in the tensile strength of the sample for 35 kGy of dosage and similarly went down to 42 MPa which is around 90% decrease in the tensile strength of the polypropylene sample when compared with the control sample. One of the reasons for this decrase could be the damage in the fiber cased by the radiation. In the SEM images of 35 kGy and 70 kGy sample as shown in Figure 16 and 18, small filaments in the yarn can be seen damaged and the extent of damage increased when the the radiation dosage is increased. Clearly, chain scission effect can be observed for the fibers when radiated with high energy radiation. However, when radiated with 5kGy of irradiation , it only limited to the disturbances created on the surface of the sample and does not damage any morphology of the sample.

`

3 FIBER PULLOUT

3.1 Introduction and Objective:

When a load is applied to the matrix, part of the load is transferred to the fiber along its surface. Because of the difference in stiffness between the fiber and the cement matrix, shear stresses develop along the surface of the fiber resulting in the development of force transfer, however as this stress is increased by higher load levels, debonding occurs which leads to shear micro cracks. Therefore, the stiffness and frictional resistance (sliding) of the fiber-matrix interface gives a measure of the toughness and strength and the effectiveness of the bond parameters.

The objective of this section is to characterize the fiber and matrix interface in terms of adhesion and frictional bond properties. The tasks developed under this program include:

1. Preparation of fiber pullout samples using different fiber parameters and matrix characteristics
2. Experimental testing of fiber pullout tests and obtaining pullout force slip response of fibers embedded in a cementitious matrix. Use the test results to obtain the load-slip response of a single fiber reinforced in cement matrix and to compare it with a theoretical model.
3. To obtain the stiffness and the resistance of the interfacial zone of fibers reinforced in cement matrix.
4. To compare the results of irradiated and non-irradiated fiber sample responses and results.

`

3.2 Pullout Literature:

3.2.1 Introduction

Load carrying capacity of cement-based composites depends on the performance of three components: fiber, matrix and the interface. The brittle matrix cracks when subjected to tensile stresses greater than its tensile strength. The occurrence of cracking is unavoidable but controllable by mean of force transfer mechanism. A well-developed bond between matrix and fiber increases force transfer between the two phases. Continuous reinforcement systems such as textiles transmit localized forces to regions far away, leading to multiple cracking. The net result is that the structural stiffness slowly degrades. On the contrary, poor bonding and discontinuous fiber reinforcement result in a few larger cracks localized in a narrow region. The stiffness degenerates more rapidly and crack widths soon become visible. Proper modeling of load transfer between the two materials is a crucial tool in the development of high performance discrete fiber and textile reinforced cement composites.

Sample Preparation procedure

`

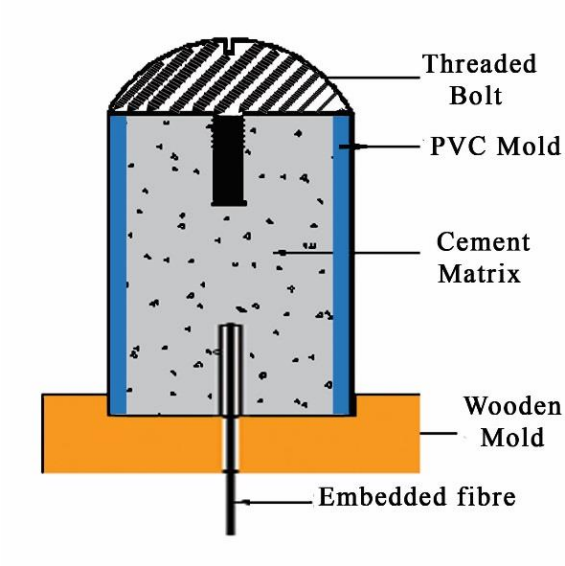

Figure 19: Schematic of the specimen before casting

Table 7. Mix formulation of matrix

Mix ID	Mix proportions	Curing (days)	Fiber Types	Fiber Embedded Length (mm)
A	1C:0.4W	7,28	Forta	19.0
B	1C:0.15 FA 0.4W	7,28	Forta	19.0

`

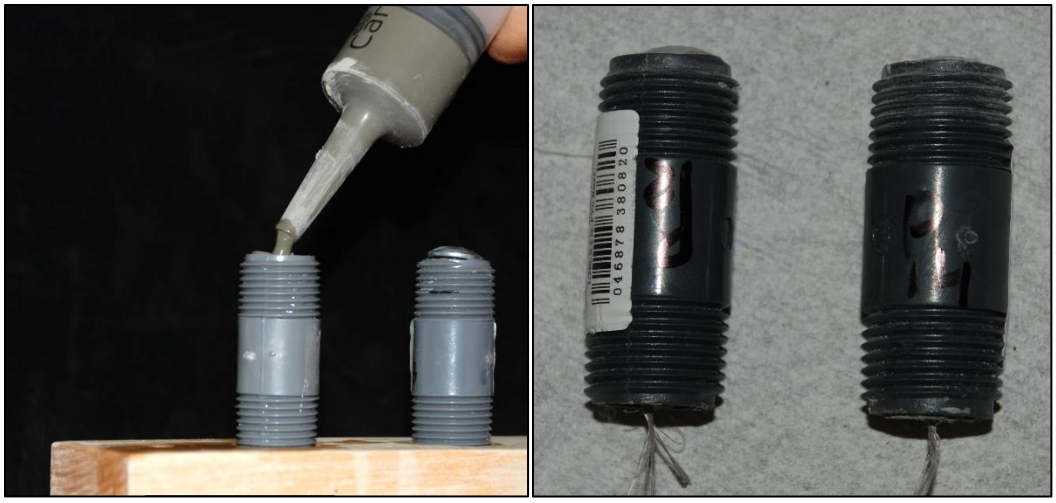

Figure 20: (a) cement matrix being poured in the PVC mold containing fiber by means of a syringe. (b) Finished Forta specimen

All specimens were cast in a PVC mold of 12.7 mm diameter, 50.8 mm height with varying embedded lengths of fibers. The specimens were cast using wooden supporting molds which held the fiber at the required embedded length and the concrete was poured after placing the sample on the wooden mold. Step by step procedure for sample preparation is as follows:

1. Clean the wooden mold and orifices before rowing the fiber through the mold.
2. Bring the fiber to the desired embedded length and secure the loose end by means of tape.
3. Once all the fibers are ready, place the PVC molds around the fibers.
4. Pour the matrix in the PVC mold using a syringe. Cover the cast sample with a threaded bolt with a rounded head to anchor the matrix on the top edge.

`

5. Remove the tape from the other end and remove the sample from the wooden mold after 24 hours of casting and cure as per the age requirement

3.3 Experimental Program

The test set up consisted of attaching the specimen while inside the mold to one end of the testing machine using a threaded screws available in the mold from one end. The other end of the free fiber length was secured in a fiber gripping hollow hole as shown in the Figure 21. This grip was used to secure the inserted loose fiber in a hole by means of three screws. A thin copper sheet was used to apply a uniform pressure along the length of anchorage the fiber in order to prevent it from failing in the grip. Tightening of the set screws resulted in distributing a grip pressure evenly on the fiber face. The bottom of the fiber embedment grip was connected to the stroke actuator using a connecting pin as shown. A 300-lb. load cell was used to record the pullout force. Tests were conducted in a MTS 810 system servo hydraulic system.

`

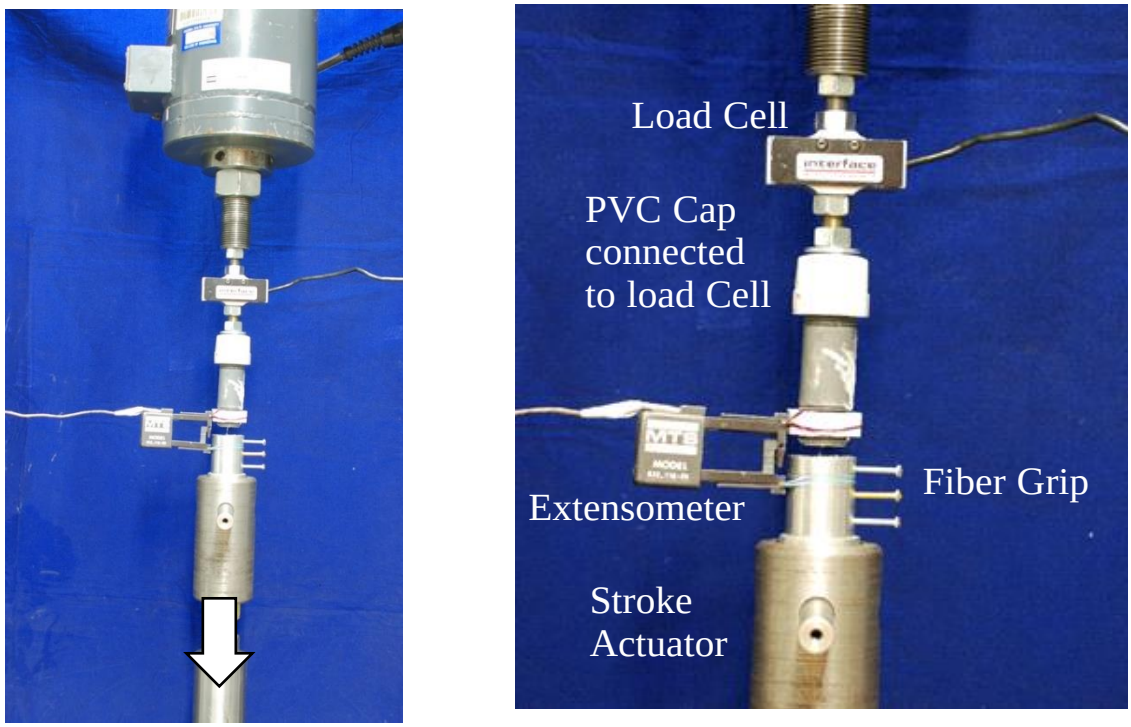

Figure 21: a) Experiment Setup on MTS 810, b) Test Setup for fiber pullout tests.

A calibration factor pf 128.86 lbs. /V was used to convert the raw data into the load cell response in force units. A 0.15-inch range of gage length extensometer was used to record the slip between the matrix and the fiber end. The extensometer was mounted using stiff rubber bands to reduce slip. The top arm was in contact with the core and the bottom arm was placed on the fiber grip thus ensuring slip of fiber from the core. The fiber was mounted close to the fiber end achieving negligible free length between the sample and fiber grip such that a true load slip curve can be obtained which will not require any correction for the free length elongation. Displacement control test at the rate of 0.1 in. /min was performed on the pullout sample.

`

3.4 Test Results:

Pullout tests were carried out on a MTS 810 at 3 different static crosshead rates of 0.1 inch/min. The experiment was at least 3 replicate plots for every sample group. Samples disturbed while setting up or misaligned tests were discarded.

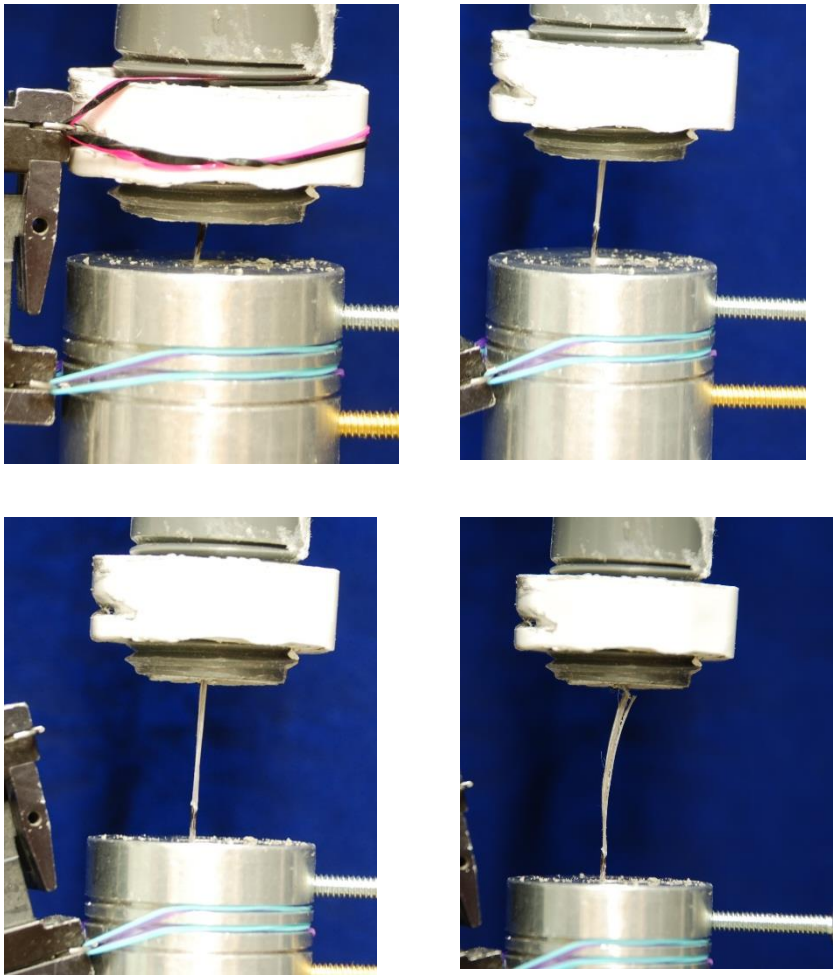

Figure 22: Fiber being pulled out as the test progresses. A, b, c, d stages of loading

The PVC core was first mounted in the threaded PVC cap and tightened to avoid any slip. The free fiber was then pulled through the fiber grip and secured by

`

means of the three screws as mentioned above. The set up was then aligned and connected to the bottom actuator. The extensometer was then attached as shown on a PVC sleeve around the core to measure the local slip of the fiber. Figure 23 shows the extensometer vs. stroke slip response. Note that there are significant spurious deformations when the stroke actuator response is measured as a component of the slip. The extensometer presents a far more accurate measurement of eth stiffness of the bond as compared to the stroke displacement. The extensometer response was used to measure the initial stiffness of the sample and the remaining parameters were estimated from the stroke response. Due to the small range of the extensometer, the test was paused and extensometer removed before the test could proceed to the end. This caused a kink in the load slip response due to fiber relaxation, which had to be accounted for while processing the data.

`

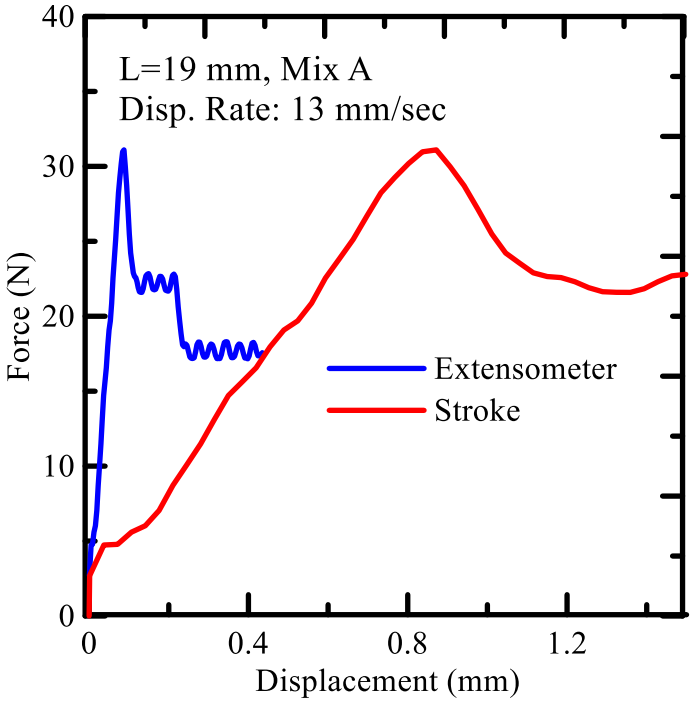

Figure 23: load slip curve response of the extensometer vs. stroke slip

Test results can be used to determine the fiber-bond stiffness, the maximum load, initial elastic stiffness of the interface, the slip at maximum load, the energy dissipated due to pullout.

3.5 Results and Discussion:

Results of the 7 days and 28-day tests are shown in the appendix of the report. Note that due to the nature of the fiber interface there is wide range of distribution among the various fibers.

`

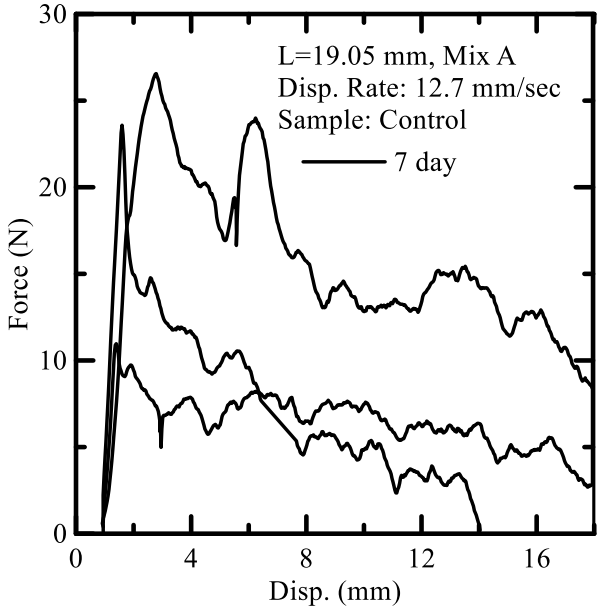

(a)

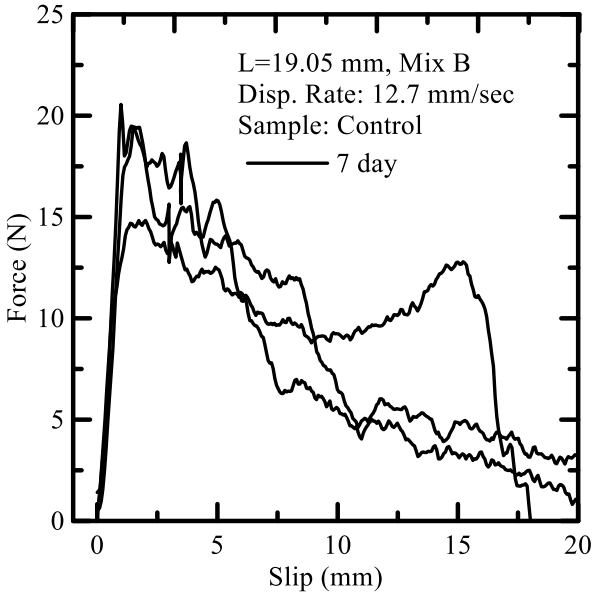

(b)

Figure 24: Control Sample, 7 Day. (a) Mix A. (b) Mix B

`

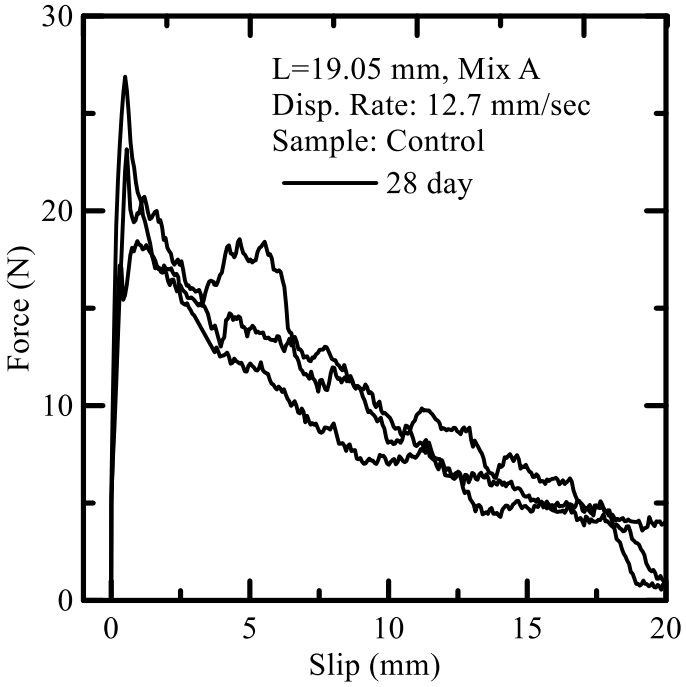

(a)

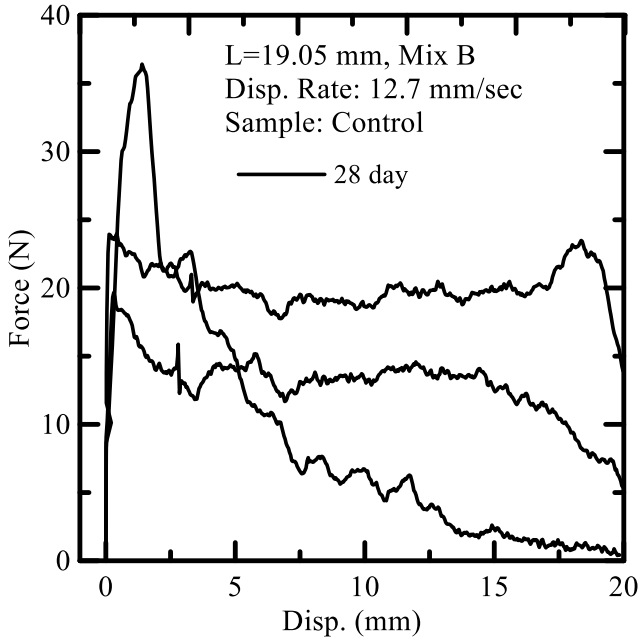

(b)

Figure 25: Control Sample, 28 Day. (a) Mix A. (b) Mix B

`

Embedded length 19.05 mm.

Table 8: Strength parameters of the tested samples.

Curing (Days)	Mix Type	Rep. ID	Max Load, N	Stiffness, N/mm	Toughness N.mm
7	A	P1	11.0		
7	A	P2	26.6	70.09	304.2
7	A	P3	12.2	41.13	113
7	A	P4	24.6	15.25	326
7	A	P5	21.8	30.01	310
Average			19.2		
Std. dev			7.2		
7	B	P1	22.6	27	347.5
7	B	P2	14.8	24.38	178.5
7	B	P3	19.5	40.77	158.6
7	B	P4	20.6	34.07	164.6
Average			19.4		
Std. dev			3.3		
28	A	P1	26.9	72.34	349.2
28	A	P2	26.8	97.42	202.1
28	A	P3	23.0	57.31	200.4
28	A	P4	14.6	52.35	219.8
28	A	P5	18.4	48.64	156.3
Average			21.9		
Std. dev			5.4		
28	B	P1	16.3	42.28	78
28	B	P2	23.9	94.69	145.3
28	B	P3	35.8	46.24	178.8
28	B	P4	19.6	55.15	216.9
Average			23.9		
Std. dev			8.5		

Table 8 represents the strength parameter obtained after analyzing the pullout results for control sample. Two different Mixes in reference to Table 7 were used to observe the response. Response was observed at two different ages, 7 day and 28 days. Clearly the average maximum load required to break the elastic bond or shear in elastic zone was

`

more for Mix B (with fly ash) as compared to Mix A (without fly ash). The maximum load recorded to break the bond was 19.4 N for mix B and 19.2 N for Mix A, 7 day and 23.9 N for Mix B and 21.9 N for Mix a, 28 days.

Similarly, the maximum pullout force for 28 days was more than that of 7 days. For Mix A.

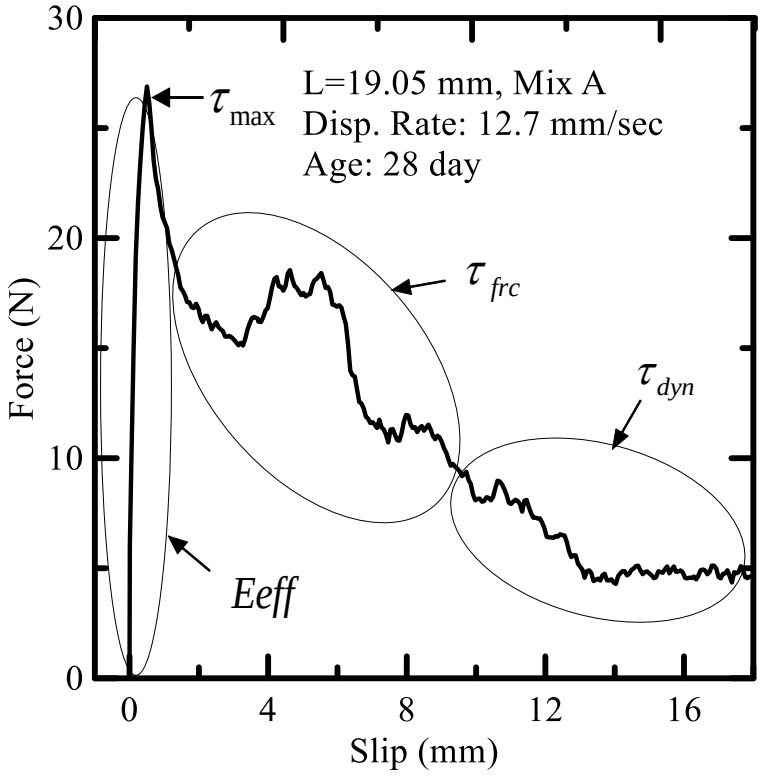

Figure 26: Phases of failure, Pullout Result.

Figure 26 explains the different stages of a pullout response of specific sample.

Energy required to pull out the embedded length of the fiber from the matrix is measured from the area enclosed in the load-slip response and can also be used as a measure to

`

characterize fiber-matrix interaction. Figure 27 represent the load slip response comparison for two different mixture, on basis of the age.

It can clearly be observed that the response of the Mix B (with fly ash) is superior to that of Mix A (without fly ash). Also, the effect of curing age on the load-slip response was observed in the study. An increase in the peak load and stiffness for 28 day cured samples was observed as compared to 7 day cured samples.

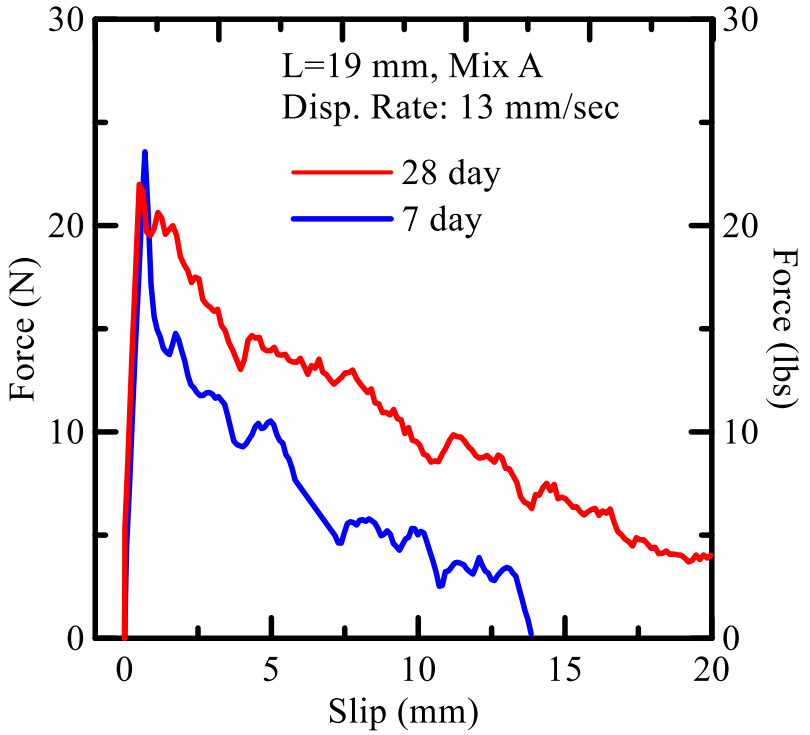

(a)

`

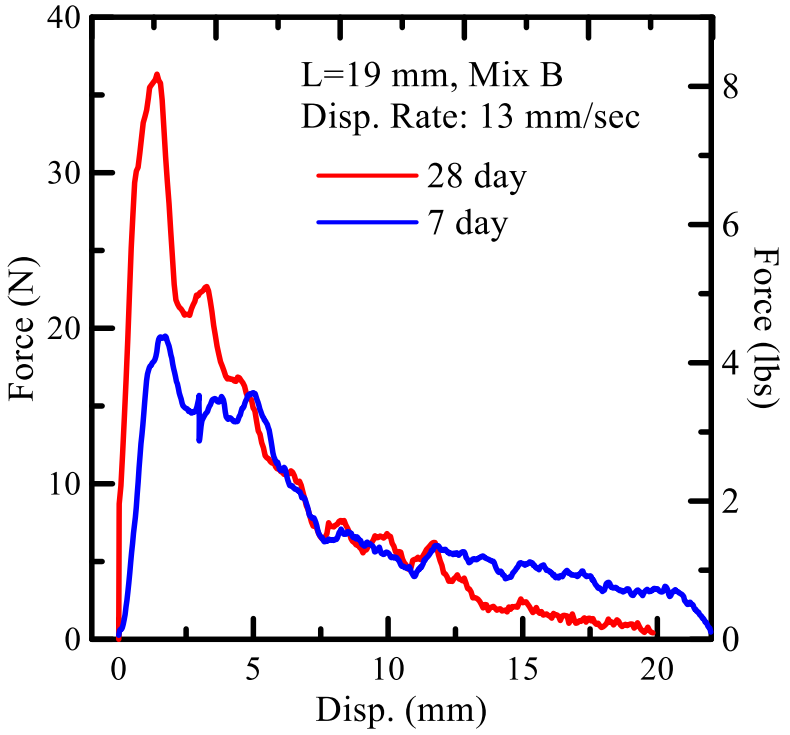

Figure 27: Comparison of 7-day vs 28-day load slip response. (a) Mix A. (b) Mix B.

`

3.5.1 Radiated Fiber Results:

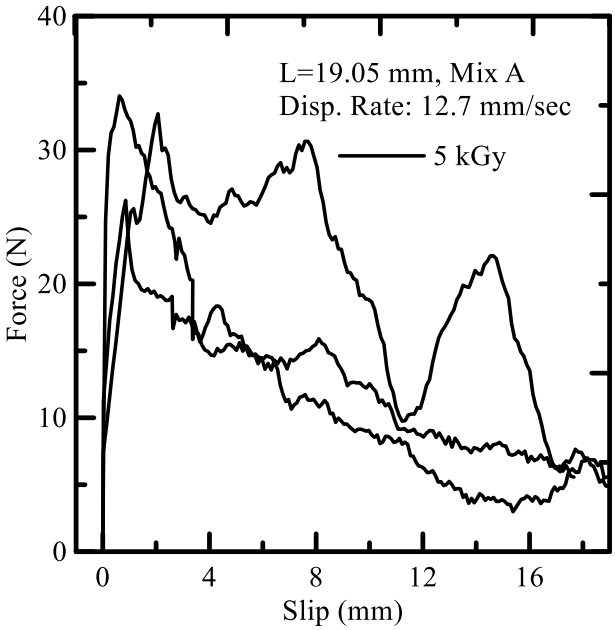

(a)

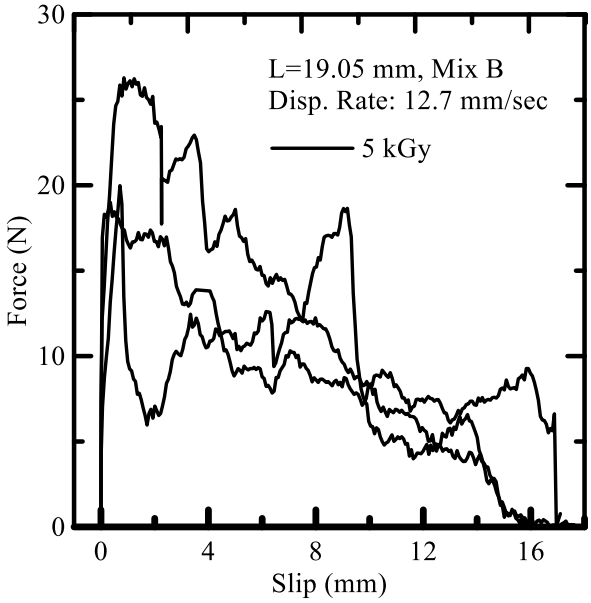

(b)

Figure 28: 5 kGy Irradiated fiber response, 7 day.(a) Mix A. (b) Mix B.

`

Table 9 : Strength parameters of the tested samples (5 kGy)

Curing	Mix	Rep. ID	Max Load A	Stiffness	Toughness
(Days)	Type		N	N/mm	N-mm
7	A	P1	32.6	19.28	374.1
7	A	P2	26.48	33.6	241
7	A	P3	28.9	78.9	52.1
Avg.			29.3	43.9	222.4
Std. dv			3.08		
7	B	P1	20.2	26.3	187.9
7	B	P2	26.6	108.4	131.2
7	B	P3	10.51	41.66	80.8
Avg.			19.1	58.8	133.3
Std. dv			8.1		

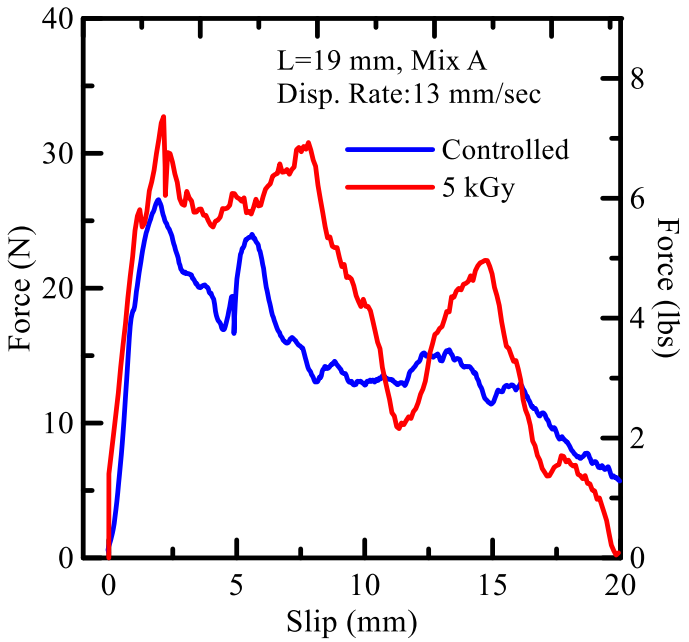

(a)

`

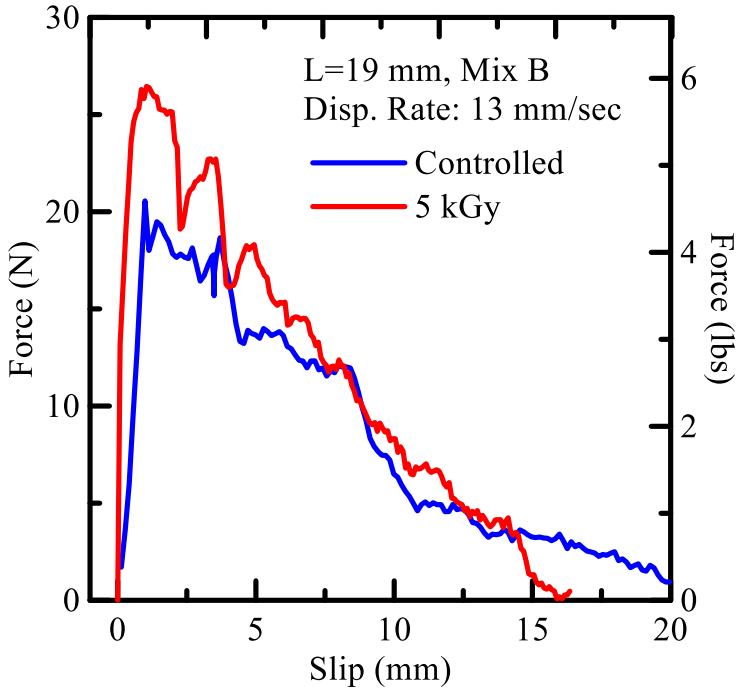

(b)

Figure 29: Comparison of controlled vs 5 kGy load slip response, 7 days. (a) Mix A. (b) Mix B

Pullout test was conducted on 5 kGy sample and the load vs slip responses of the samples are shown in Figure 28. The comparison of the irradiated and non-irradiated is shown in Figure 29. We can observe an increase in the stiffness of the pullout sample after it is being radiated with 5 kGy of dose. A minimal increase in the peak load was also observed for the 5 kGy sample when compared to controlled sample.

Pullout test was also conducted on 35 kGy and 70kGy samples. However, fibers failed even before the matrix failure. The results of the 35 kGy is shown in Figure 31. It can clearly observe from the load vs slip behavior a very low peak load following the fiber

`

failure, without any matrix failure. Two inferences can be taken out from this result, either an increase in the maximum shear bond strength have caused this failure or decrease a decrease in the tensile strength of the fiber. Similar failure pattern was obtained for 70 kGy sample.

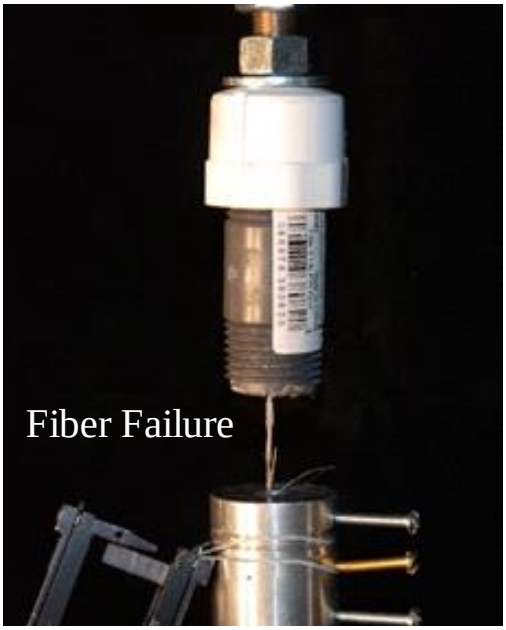

Figure 30: 35 kGy sample illustrating fiber failure before matrix failure.

`

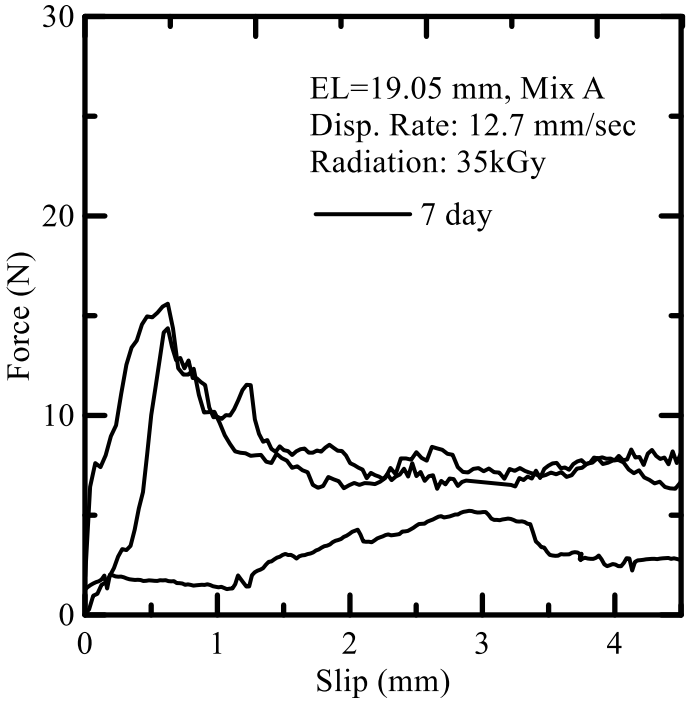

Figure 31: Data points to illustrate the response (35 kGy)

3.6 Significance of Interfacial Modeling

As the pullout responses varies a lot it becomes necessary to simulate it to a model which could average the over response for a set of samples. Also, simulation gives more insight to different parameters responsible for the pullout failure.

The stiffness of fiber-interface-matrix system directly affects the toughening mechanisms. In brittle matrix composites, if the ultimate strain capacity of the fibers exceeds that of the matrix, fibers will bridge matrix cracks. The force transferred due to the bridging reduces the stress intensity factor at the tip of the matrix crack. The constitutive response of the debonding phase depends on the length of cylindrical or

`

planar shear micro cracks which form at the interface, and the ability of the interface to transmit the traction across a matrix crack. For properly designed systems, matrix's tolerance to the crack propagation and thus composite strength may increase significantly as shown by Aveston, Cooper, and Kelly [26], and Kelly and Tyson [27]. The fibers bridge across the matrix cracks and processes of debonding and pullout lead to toughening and energy dissipation.

Several fiber pullout models have been proposed to characterize bond properties of single fibers with a cementitious matrix. One of the main justifications for modeling of pullout mechanisms is to better address closing pressure formulations. The distribution of the traction force over the crack length depends on the interaction of the debonding fibers with the matrix crack in an opening mode. Closing pressure formulations have been modeled by several approaches including closing pressure forms that are square root dependent on the fiber slip [28][29], and correlate the fiber, matrix, and interface properties to the composite response including the work of McCartney [30], Budiansky et al. [31], and Marshall et al. [32].

A variety of analytical solutions [33,34,35] assume that while fiber and interface behave elastically in bonded regions, a constant residual shear strength is in the debonded region. Bond strength models for rebars also address the pre- and post-peak response [36,37]; however, the more detailed the bond strength model, the more complex the analytical solution. Currently, most bond properties of the textile structure are obtained from straight fiber pullout which treat textile (grid reinforcement) as an equivalent smooth longitudinal fiber.

`

Modeling of the failure process at the interface requires numerical simulation of the stiffness degradation before peak load using a formulation for stable propagation of debonded zone. Interface toughness and frictional sliding resistance can be measured by curve fitting the load-slip response using micromechanical models. Theoretical load-slip response can be obtained using stress based, or crack growth fracture criteria. The available modeling schemes are based on a variety of analytical, finite element, and finite difference techniques. Two approaches of shear strength and fracture mechanics criterions are commonly used in the analysis of pullout tests [38]. The simplest models that are reasonably accurate, assume that sliding along a debonded interface is governed by a constant shear stress, τ, [39][40][41]. Coulomb friction law has been used to study the effects of residual and thermal stresses ([42][43] [44]. Ballarini et. al. [45] and Mital and Chamis [46] carried out finite element studies using the Coulomb friction law.

Pullout of straight yarns is based on the shear lag approach which includes frictional and adhesion bond. The pullout force vs. slip displacement is obtained using a sliding contact surface to model debonding and slip. The debonding criterion is defined using the interfacial strength. After debonding, Coulomb friction is introduced in the debonded zone to account for interlocking effects. This simulation provides theoretical pullout response as affected by the parameters of interface as it is calibrated with experimental pullout results.

`

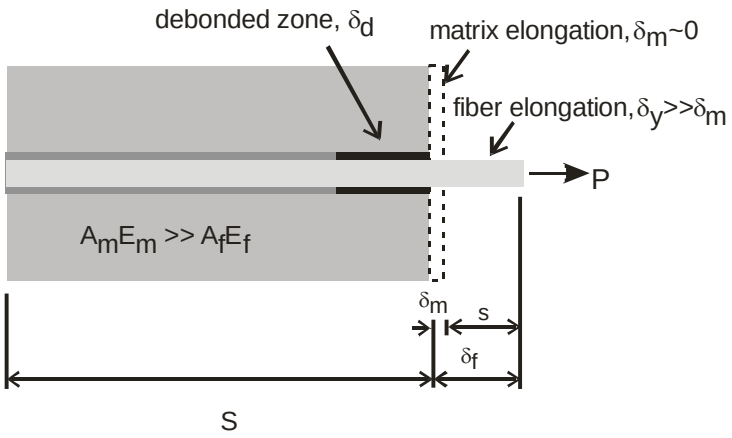

Figure 32: Pullout-Slip and the various zones of bonded, debonded, and sliding interface.

3.6.1 Pullout Tests

A variety of pullout tests have been developed. Figure 32 shows the schematics of test parameters during a pullout-slip test. Various zones of interface include: bonded, debonded, and sliding. Using the complete load-slip response, stiffness of the interfacial zone and the shear strength parameters can be obtained by using a standard fiber pullout model. In a pullout test by Li et al. [47], fiber debonding under slip controlled closed-loop tests was measured. Test methods have also been developed to characterize the pullout response of fibers from a portland cement matrix [48]. Due to fibrillated nature of polymeric fibers, determining perimeters using digital analysis of images captured from thin sections, one can obtain the effective perimeter parameter and use this to characterize and optimize the bond and fiber length parameters [49].

`

3.6.2 Analytical Derivation for Fiber Pullout

A pullout model to characterize the parameters of fiber and textile-cement systems is presented in this section. The derivation is similar to the single fiber analogy of Naaman [50] [51]. The first set of solutions allow for comparison with fiber composites. In the case of fabrics, effect of transverse yarns is included using additional terms to address the bond contributions due to orthogonal fill yarns. The geometrical interlock of a textile system into apparent chemical and mechanical bond characteristics results in overestimation of bond properties.

The characteristic of the curve as shown in Figure 32 can be divided in into various stages of stress distribution in the fiber. Initially, the linear response corresponds to perfect bonding of fiber and the cement paste. At certain point on the ascending curve, the response becomes nonlinear due to some parts of the fiber starts debonding and propagates along the embedded length. This causes strength softening on the ascending curve until it reaches the maximum strength. The debonding continue in the post peak region and until the entire length becomes debonded and then the fiber starts to slide out dynamically. There are therefore 3 stages: elastic, nonlinear and dynamic. The derivations along with the assumed shear stress and force distribution for each stage will be explained in the next section.

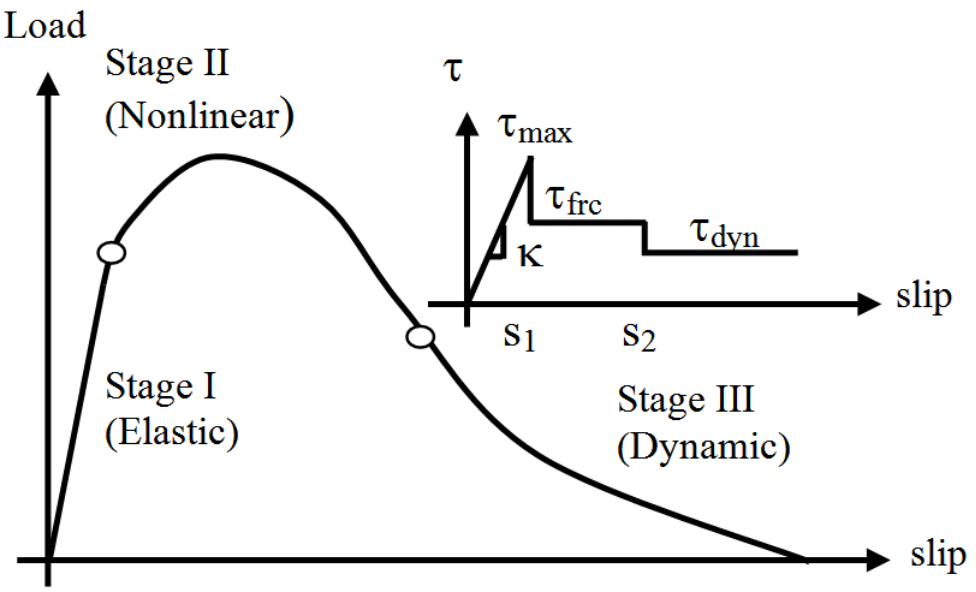

Figure 33: Pullout-Slip Response and Shear Strength Diagram

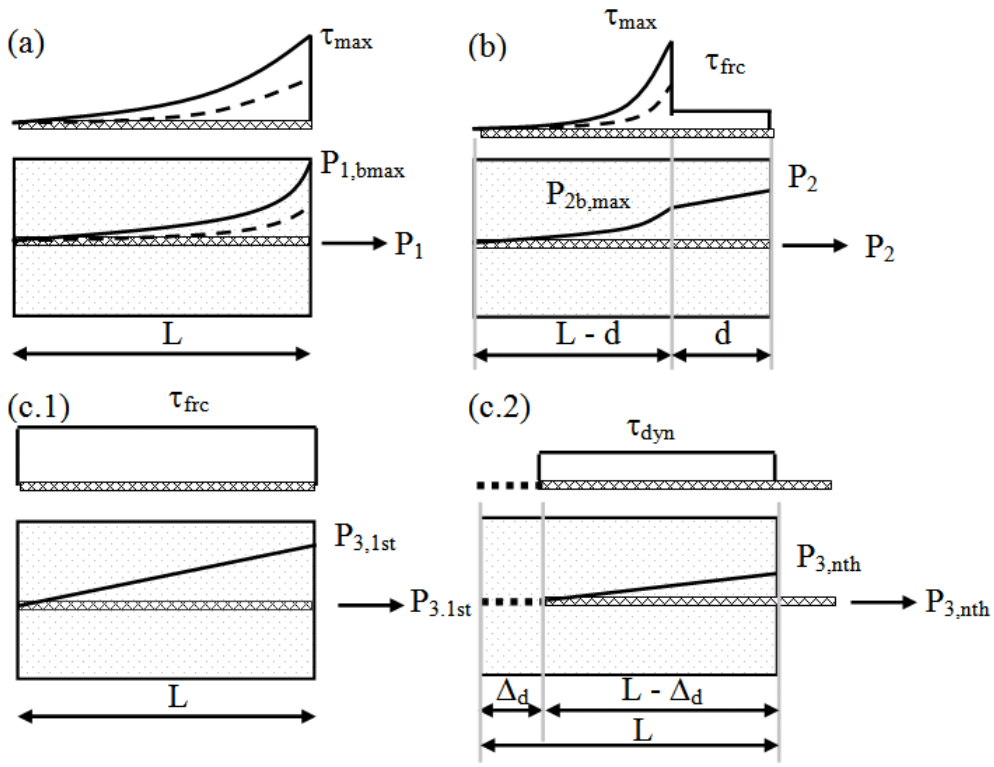

`

Figure 34: Shear Stress and Force Distribution along the Yarn: (a) Stage I (Elastic Response); b) debonding, c) frictional pullout, and d) sliding mode.

Pullout Response in Elastic Stage (I)

As long as the shear stress at interface is less than the maximum shear strength τ_{max}, yarn and matrix are fully bonded the applied load is less than the maximum bonded load $(P_1 < P_{1b,max})$, and standard shear lag solutions apply.

Pullout Response in Nonlinear Stage (II)

After loading beyond the elastic limit, debonding at the right end starts and extends by a distance d, with a frictional shear strength τ_{frc} while on the left portion $(L-d)$, the two materials are still perfectly bonded. The criteria for the growth of debonding is specified as a shear strength criterion with a constant frictional stress along the debonded zone, in addition to a shear lag model terminating with τ_{max} at the debonding junction.

Pullout Response in Dynamic Stage (III)

The dynamic response of the pullout in the third stage consists of two conditions: initial stage up to complete debonding and rigid body motion. It is assumed that up until the yarn is completely debonded, the shear resistance still remains τ_{frc}. Upon the completion of debonding, no sliding has occurs $(\Delta_d = 0)$ until the yarn begins rigid body motion. As the yarn starts to slide by a distance $\Delta_d > 0$ the resisting shear stress is assumed to drop to dynamic shear strength τ_{dyn}. During the Initial stage ($\Delta_d = 0$), the shear resistance is uniform τ_{frc} throughout the yarn length, resulting slip at the end of the yarn in the initial stage is obtained in a same way as the initial case. During the rigid body motion stage

`

($\Delta_d > 0$), shear resistance drops to τ_{dyn} and the embedded length reduces to *($L-\Delta_d$)*. The measured slip is computed as an additive portion of end of stage II (static) $S(L)_{2,last}$ and the slip in stage III rigid body motion mode.

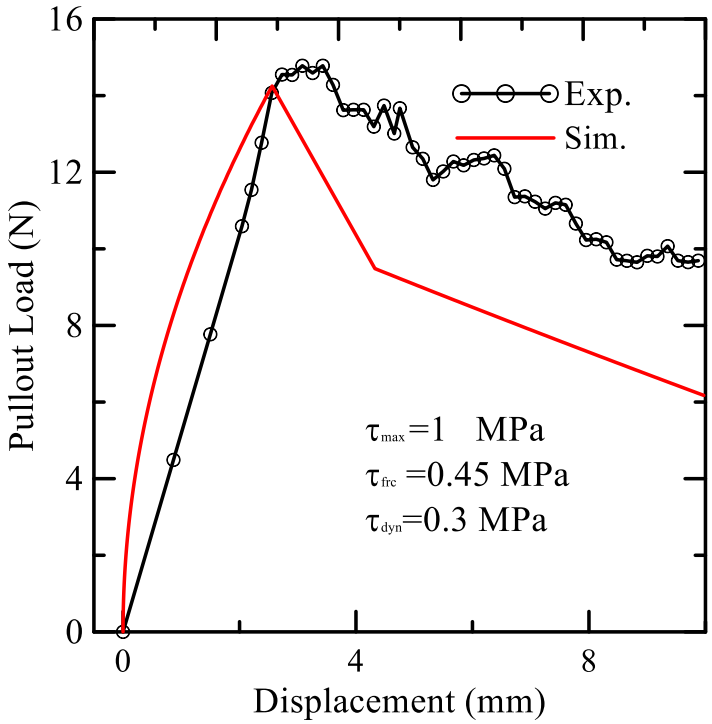

(a)

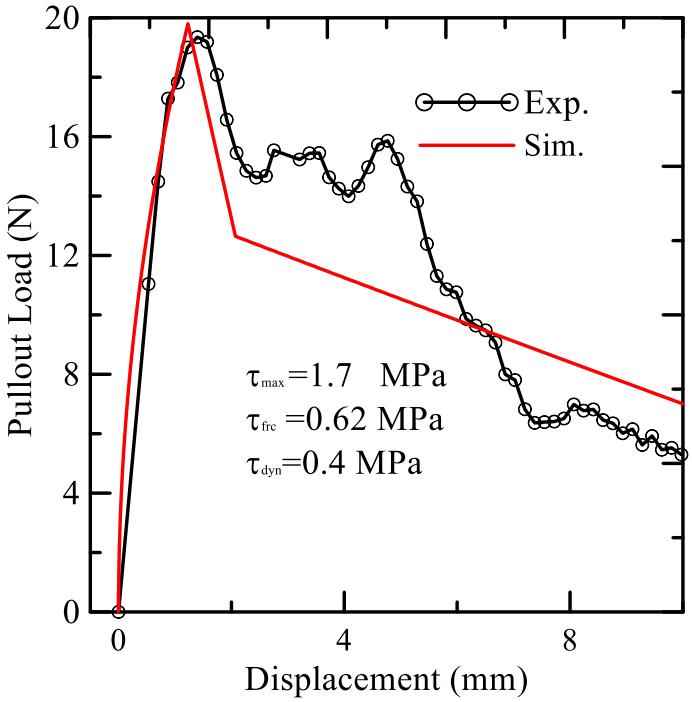
Exp.
Sim.
τmax=1.7 MPa
τfrc =0.62 MPa
τdyn=0.4 MPa
Pullout Load (N)
Displacement (mm)
0
4
8
0
4
8
12
16
20

(b)

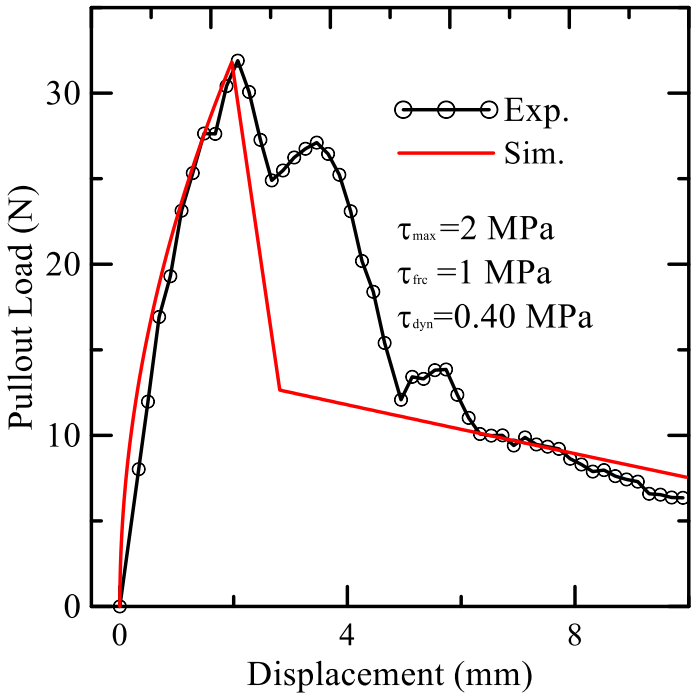
Exp.
Sim.
τmax=2 MPa
τfrc =1 MPa
τdyn=0.40 MPa
Pullout Load (N)
Displacement (mm)
0
4
8
0
10
20
30

`

(c)

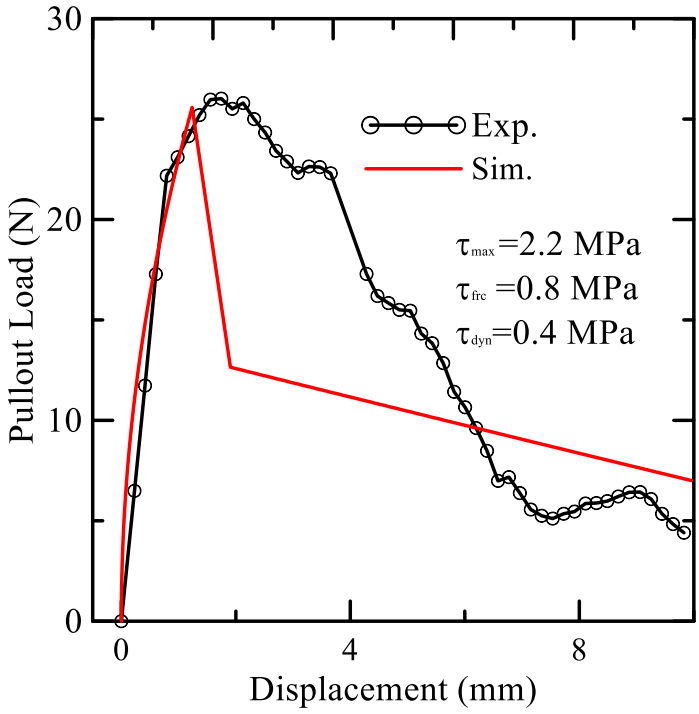

(d)

Figure 35: 7 day Sample Pullout Simulation results. Embedded Length: 19 mm and Disp. Rate: 13 mm/min.

As it can be observed from Figure 35 that there is an variability in the response of pullout results. τ_{max}, τ_{frc}, τ_{dyn} represent the shear stress at three different stages of pullout response. τ_{max}, represent the shear stress at maximum pullout load. The values of τmax for different samples as shown in Figure 35 varies from 1-2.2 MPa. Similarly,τ_{frc} and τdyn represent the shear at friction which represent the stage 2 and shear stress in the dynamic

`

zone (Stage 3). Values of τ_{frc} and τ_{dyn} vary from 0.45 to 1 MPa and that for dynamic zones 0.4 MPa. Stress value did not vary much for the peak and dynamic loading but the variation in the shear friction was large. This could be because of the fibrillation nature of the fiber. So, it became necessary to simulate all the results for one value and come up with one τ_{max}, τ_{frc} and τ_{dyn} value. Single simulation for all the sample presented in Figure 35. To show the bilinear response of the model untill the peak load the plot was only shown till the peak load, for the slip or displacement untill 2.5 mm.

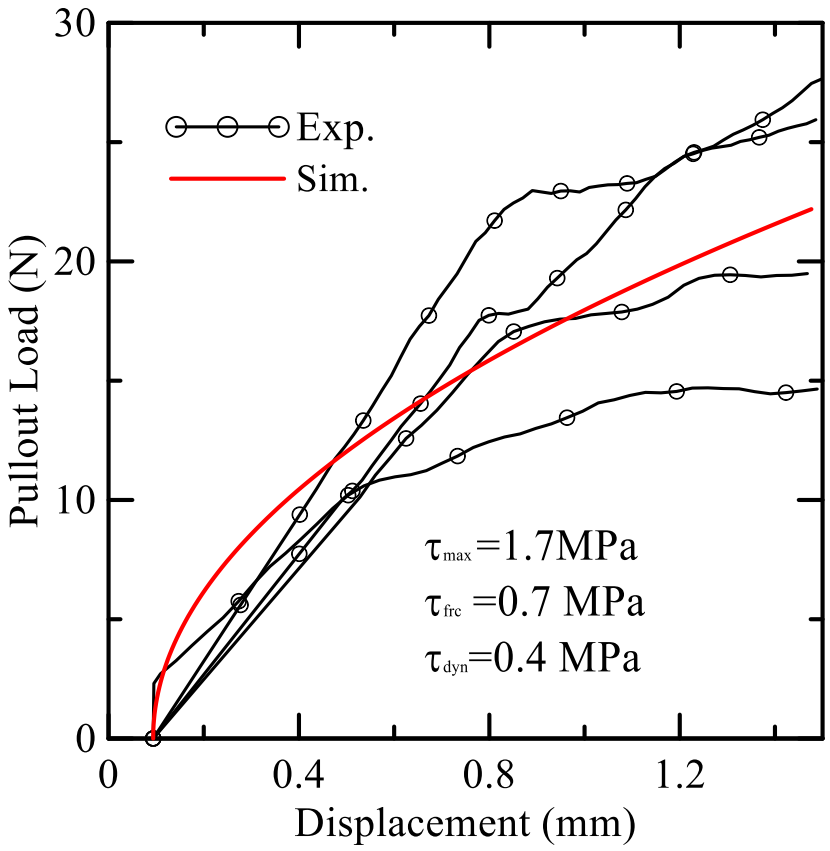

Figure 36: 7-day pullout simulation.

`

4 FLEXURAL TESTS ON FIBER REINFORCED MORTAR

4.1 Four-point bending tests.

Standard four-point bending tests were performed on six replicate Forta FRC beams pertaining to the mix design mentioned in appendix. The test setup before and after the test is shown in LVDT is mounted on the back face of the beam to measure the axial deflection of the beam. The testing procedure used for running these tests is summarized in Table 10. As evident, the complete procedure is split into three phases based on the mode of control during the test.

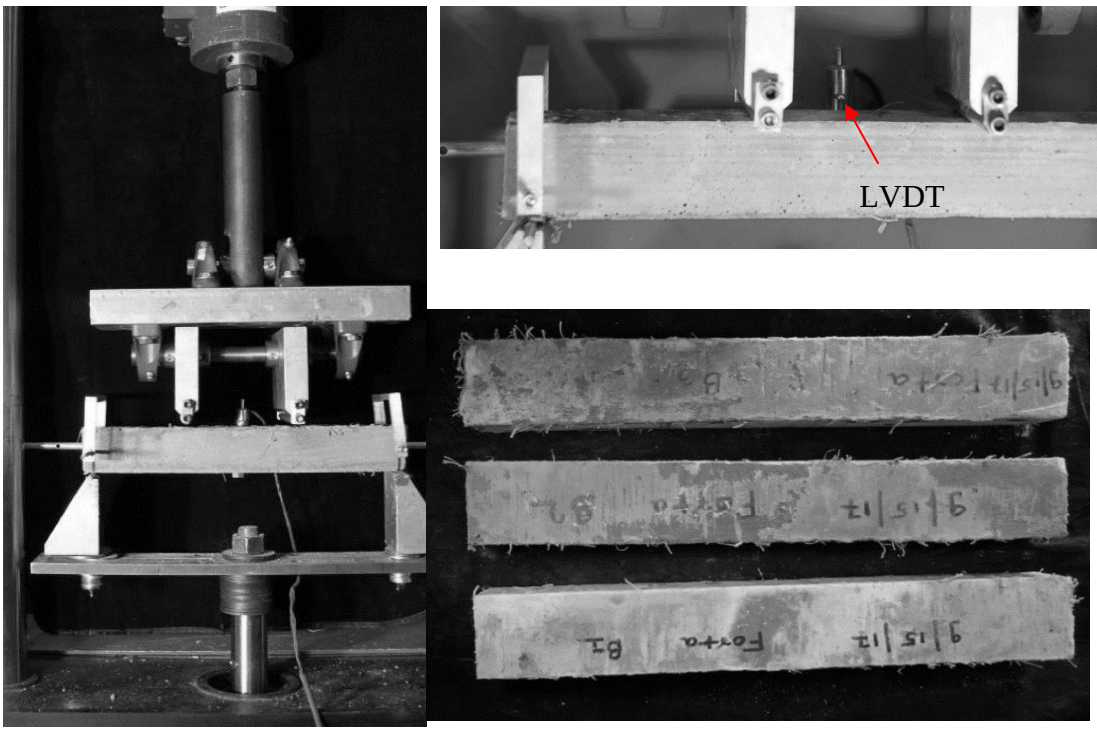

Figure 37: Experimental setup & samples used for running the standard four-point bending tests.

`

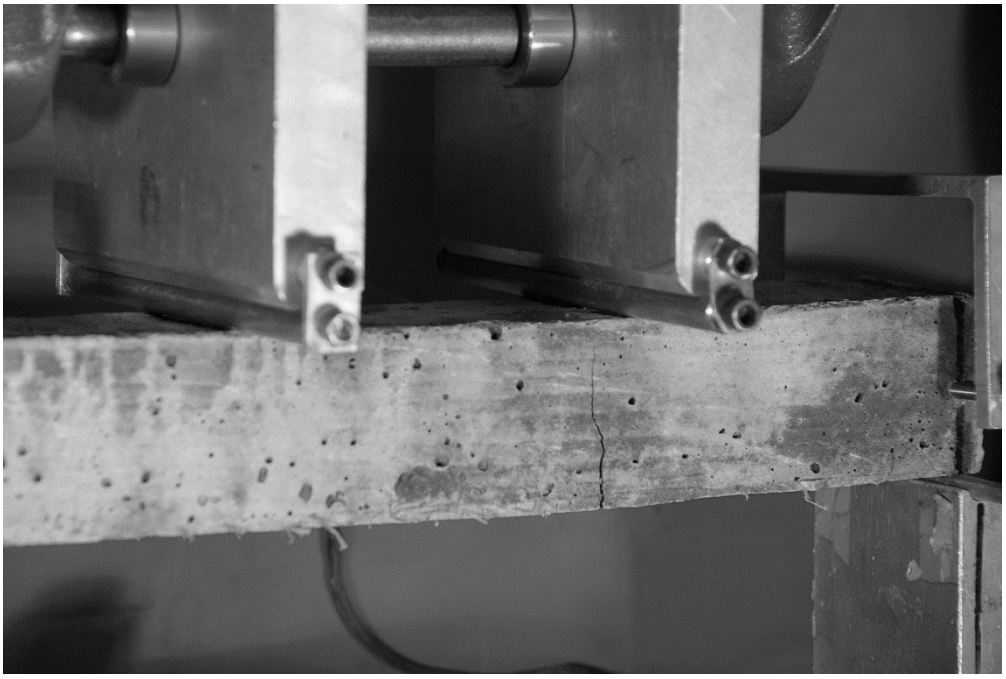

Figure 38: FRC beam specimen after testing.

Table 10: Testing procedure used in the MTS station manager to control the test

Phase	Control Mode	Loading Rate	Phase Limit
1	Load	37 N/sec	6700 N
2	Actuator (Deflection)	5 μm/sec	5 mm
3	Actuator (Deflection)	20 μm/sec	7.5mm

Deflection response was measured using LVDT. The spring-loaded LVDT used in this experimental has considerably higher capacity of 7.5 mm and is hence used for parameter estimations required by ASTM 1609 testing standard, such as residual strength and toughness. Load-deformation responses of all specimens are summarized in Figure 39.

`

As evident in one of the curves, load-deflection curve is terminated before 3 mm, which is equivalent to deflection limit of L/150.

4.2 Experimental responses of all beam replicate

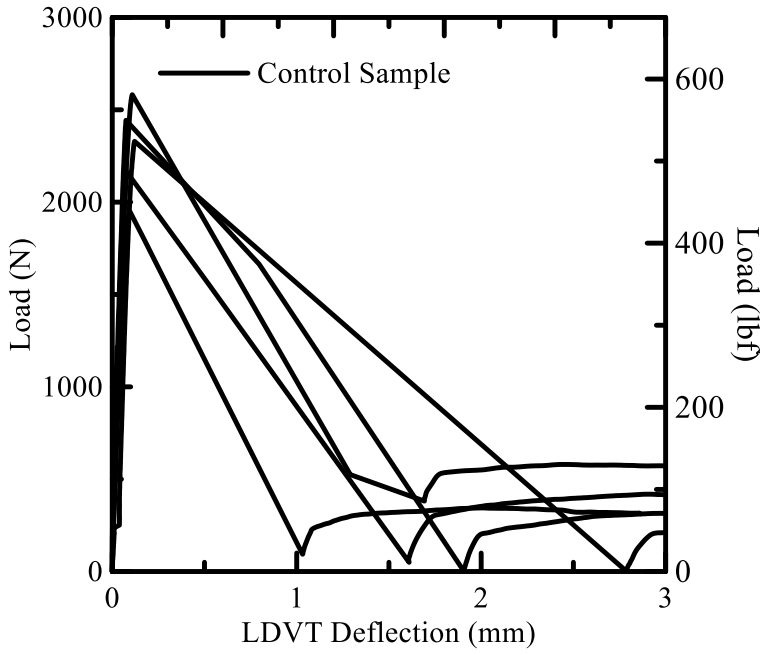

(a)

`

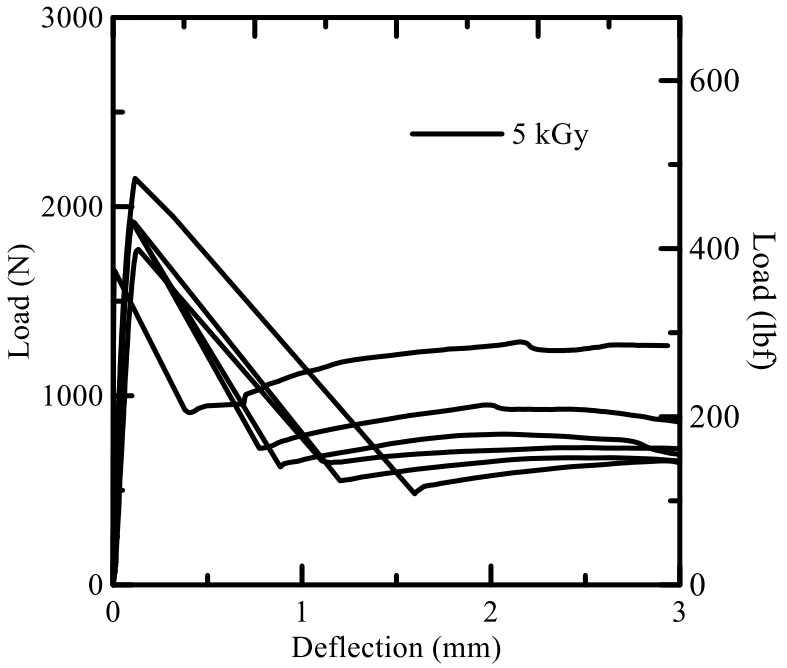

(b)

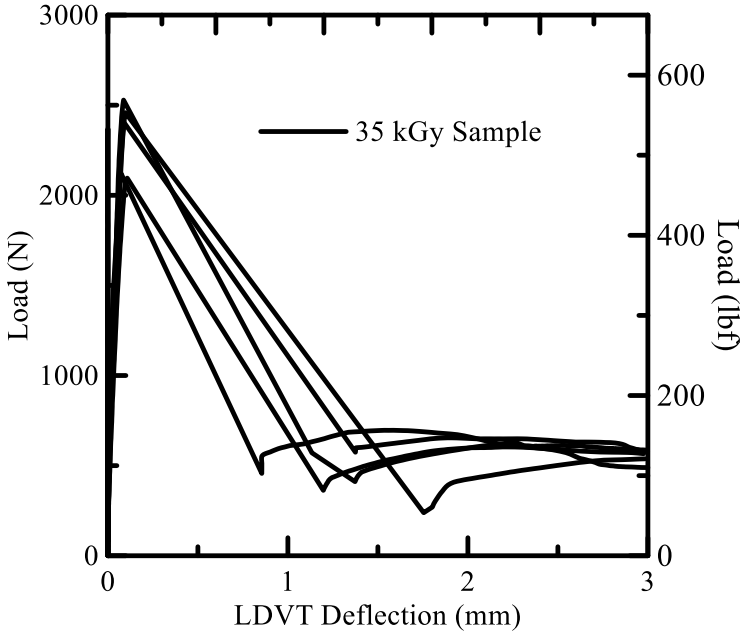

(c)

Figure 39: Mid-span LDVT deflection Vs. Loading: (a) Control. (b) 5 kGy (c) 35 kGy (d) 70 kG

`

Table A-2 and Figure 39 summarize the results of the flexural test. It can be observed that a very low residual strength is observed for control (non-radiated) sample. However, when the irradiated fibers are used in the mix we observe an increase in post peak strength which can be evidently observed from Figure 39. The increase in the post peak residual strength is more for 5 kGy sample as compared to that for 35 kGy sample. The residual strength of the control sample was in the range 200 N and that for the 5kGy & 35kGy sample is 1000 N and 500 N respectively. Clearly the roughness or the disturbance created by the radiation on the surface of the fiber has contributed to an increase in its post peak behavioral response. From the response obtained as shown in Figure 39, back calculation Excel sheet was used to obtain ASTM 1609 parameters. This can give a clearer idea effect of radiation on fiber matrix bond. From Table A-2 it can be observed that there is an increase in the residual stress values for 5 kGy as compared to control and 35 kGy sample. Value of residual stress for the sample at L/600 increased from 0.7 MPa (Control) to 1.3 and 1.2 MPa respectively. Similar increase was observed for toughness is a measure of energy absorption capacity of the test specimen. Toughness values increased from 0.69 J (Control) to 1.4 J and 1.13 J for 5 and 35 kGy samples. The peak strength has little direct relevance to fiber reinforced concrete performance. Mix design and dimension of beam plays an important role in the peak strength of concrete. After peak or residual strength is more of concern in analysis for the performance of fiber matrix.

`

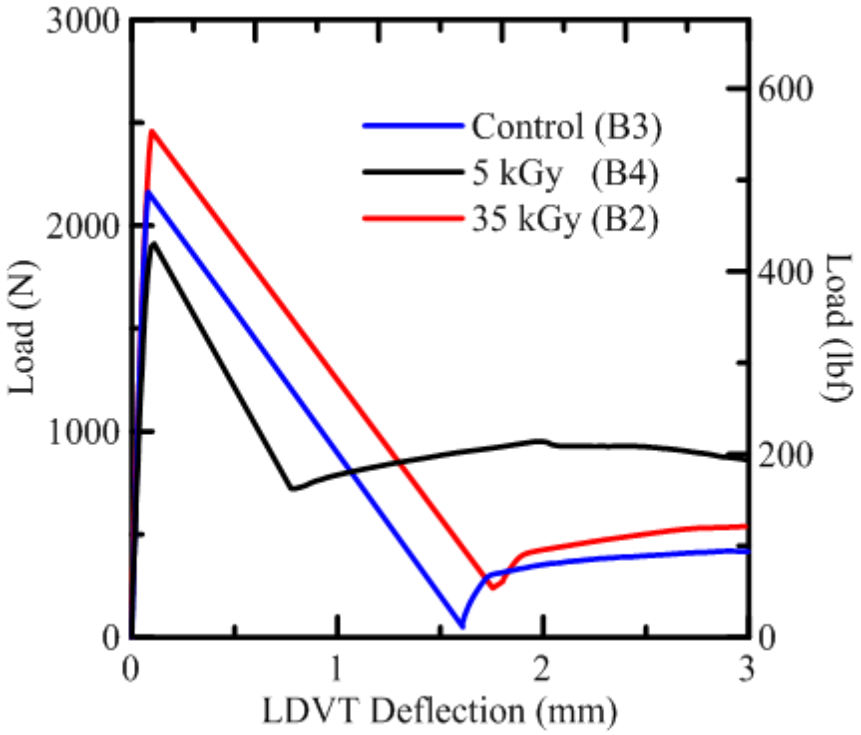

Figure 40: Sample comparison of result.

4.3 Analysis and Simulation of data:

The research team at ASU has been extensively involved in the development, design, analysis, and field work with fiber reinforced concrete as the sustainable material. Not all loading cases, applications, and specifications can be translated into compressive strength values of concrete; hence this parameter cannot be used as the sole measure of structural analysis, design, quality, and performance. It is shown that by using the newly developed design methodology, one can use fibers for improving ductility in tensile regions. Stress and strain variations introduced previously by ACI for design of unreinforced and reinforced concrete sections are shown in Figure 41. This work has culminated in a series of newly developed formulations for simplified design and analysis procedures

`

incorporating the more reliable stress-strain relationship based on the material behavior. Figure 42 shows the stress model in compression and tension for a fiber reinforced concrete section. Several publications in this area have been already adopted by the American Concrete Institute ACI-544 as design guides for use of fiber reinforced concrete.

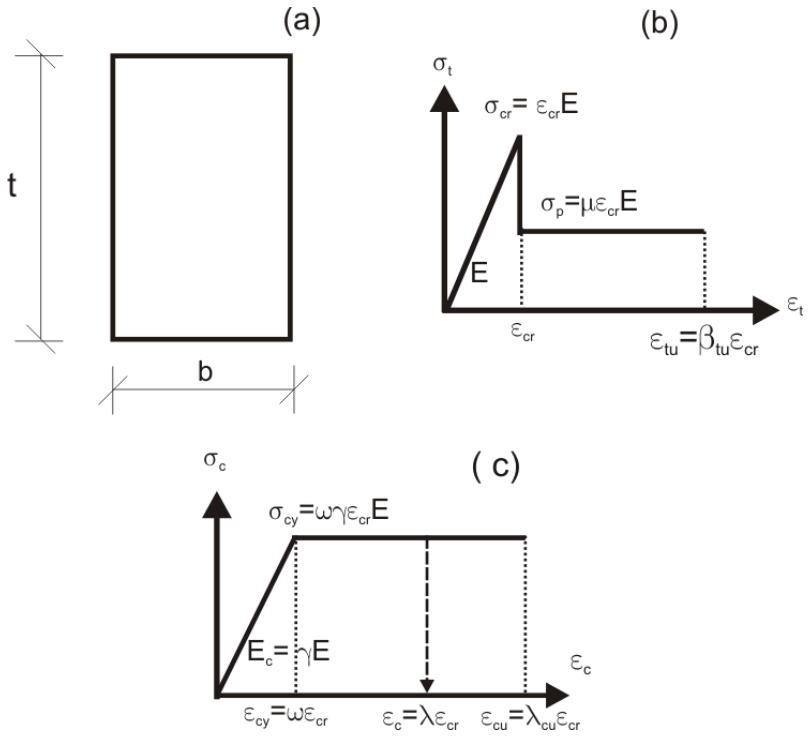

Figure 41**:** Material models for a fiber reinforced concrete section without re-bar developed in ASU (a) rectangular cross section; (b) tension model; (c) compression model.

`

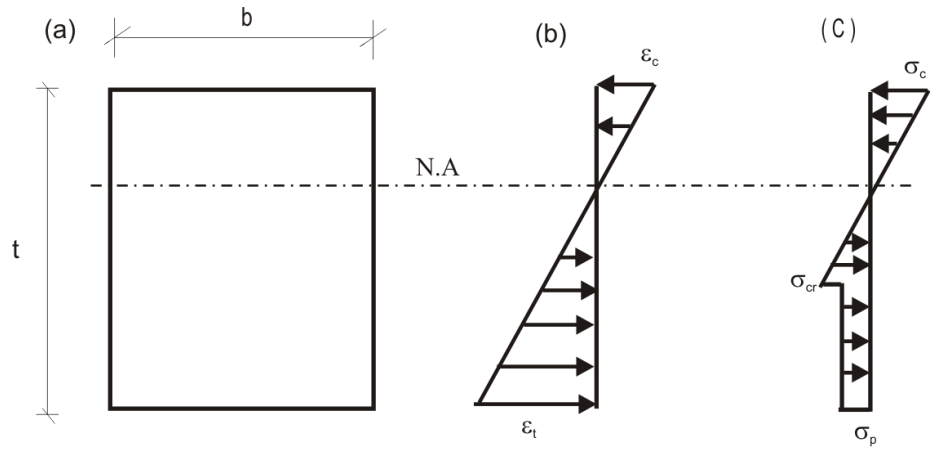

Figure 42: A rectangular fiber reinforced concrete section and the simplified strain and stress variations in bending based on ASU model.

Tension model for FRC

As shown in Fig. 34 for FRC, stress increases linearly from zero to the cracking tensile strength σ_{cr} at cracking strain ε_{cr}. Then stress drops to the constant post crack strength σ_p until it is terminated at the ultimate tensile strain ε_{tu}. Two normalized material parameters for the tension model are defined as follows:

$$\mu = \frac{\sigma_p}{E\varepsilon_{cr}} = \frac{\sigma_p}{\sigma_{cr}} \tag{3}$$

$$\beta_{tu} = \frac{\varepsilon_{tu}}{\varepsilon_{cr}} \tag{4}$$

`

Where μ is the normalized post crack tensile strength and β_{tu} is the normalized ultimate tensile strain. For SFRC system, the ultimate tensile strain is defined as 0.025 according to RILEM model [52]. Cracking tensile strength and Young's modulus can be estimated according to ACI Sec. 11.2 and Sec. 8.5.1, respectively.

$$\sigma_{cr} = 6.7\sqrt{f_c'} \tag{5}$$

$$E = 57,000\sqrt{f_c'} \tag{6}$$

Cracking tensile strain can then be calculated from Eqs. (5) and (6) as follows:

$$\varepsilon_{cr} = \frac{\sigma_{cr}}{E} \tag{7}$$

Tensile stress strain model can be obtained directly from uniaxial tension test. However, the test procedure is rather time consuming and difficult to perform. In addition, using uniaxial tensile response normally under-predict the flexural strength of strain softening FRC due to the size effect between uniform stress in direct tension test and gradient stress in bending test [53,54,55].

Figure 43 shows a uniaxial parametrized model for fiber reinforced concrete (FRC) composite with two intrinsic material parameters: Elastic modulus, E, (equal in tension and compression) and first cracking tensile strain, ε_{cr}. All strains in the models are normalized with respect to ε_{cr}. Two non-dimensional parameters: normalized post peak tensile strength μ, and compressive to tensile strength ratio ω, are also defined:

`

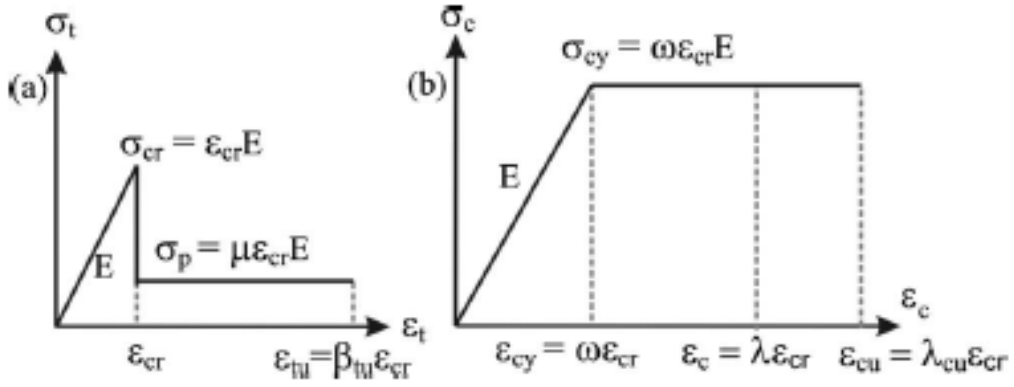

Figure 43- The Stress Strain response for tension and compression response of Fiber Reinforced Concrete according to Soranakom-Mobasher Model

The moment and curvature at any strain level (M, ϕ) are normalized with respect to their respective values at cracking (M_{cr}, ϕ_{cr}) and expressed in normalized forms (M', ϕ')

$M(\lambda,k,\omega,\mu) = M_{cr}M'(\lambda,k,\omega,\mu)$ Where $M_{cr} = \frac{1}{6}bd^2E\varepsilon_{cr}$

$\phi(\lambda,k,\omega,\mu) = \phi_{cr}\phi'(\lambda,k,\omega,\mu)$ Where $\phi_{cr} = \frac{2\varepsilon_{cr}}{d}$

`

Table 11: Parametric Definition

λ = Normalized compressive strain $\lambda = \frac{\varepsilon_c}{\varepsilon_{cr}}$ Three Stages - $(0 < \lambda \le 1)$ $(1 < \lambda \le \omega)$ $(\lambda > \omega)$	μ = Normalized post peak tensile strength $\mu = \frac{Post\ peak\ tensile\ strength}{cracking\ tensile\ strength} = \frac{\sigma_p}{\sigma_{cr}}$
ω = Compressive to tensile strength ratio	k = Neutral axis depth ratio

Table 12 summarizes the closed-form solutions for k, M', and ϕ' as these terms refer to dimensionless quantities representing the normalized neutral axis depth, moment, and curvature for the three stages of top compressive strains. The normalization constants are values that are computed at first tensile cracking ($\varepsilon_c = \varepsilon_{cr}$ or $\lambda = 1$).

The three stages are –

$(0 < \lambda \le 1)$ – Elastic for compression and tension

$(1 < \lambda \le \omega)$ – Elastic for compression but nonlinear for tension

$(\omega < \lambda \le \lambda_{cu})$ – Plastic for compression and nonlinear for tension

`

Table 12: Solutions for k, M' and ϕ'

Stage	k	M'	$\emptyset'$
$0 < \lambda \leq 1$	$\frac{1}{2}$	$\frac{\lambda}{2k}$	$\frac{\lambda}{2k}$
$1 < \lambda \leq \omega$	$\frac{2\mu\lambda}{\lambda^2 + 2\mu(\lambda+1) - 1}$	$\frac{\left(2\lambda^3 + 3\mu\lambda^2 - 3\mu + 2\right)k^2}{\lambda^2} - 3\mu(2k-1)$	
$\omega < \lambda \leq \lambda_{cu}$	$\frac{2\mu\lambda}{-\omega^2 + 2\lambda(\omega+\mu) + 2\mu - 1}$	$\frac{\left(3\omega\lambda^2 - \omega^3 + 3\mu\lambda^2 - 3\mu + 2\right)k^2}{\lambda^2} - 3\mu(2k-1)$	

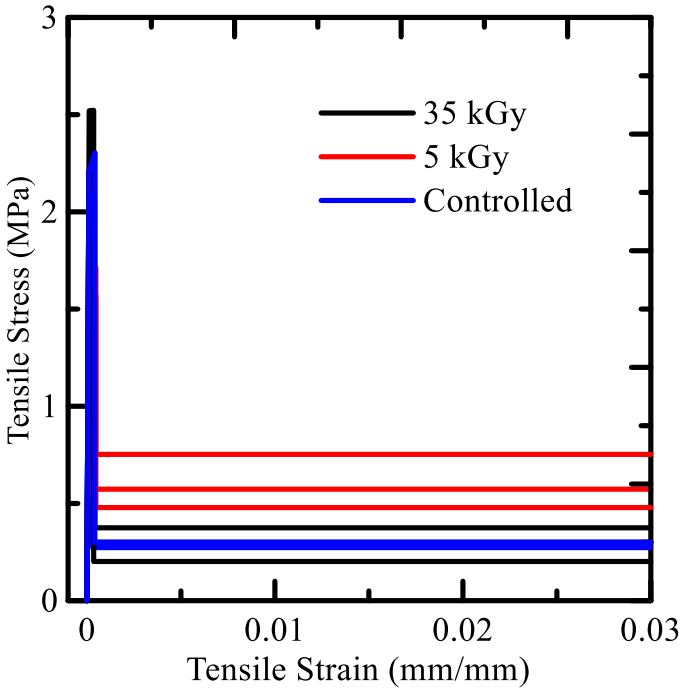
35 kGy
5 kGy
Controlled
Tensile Stress (MPa)
Tensile Strain (mm/mm)
0
1
2
3
0
0.01
0.02
0.03

(a)

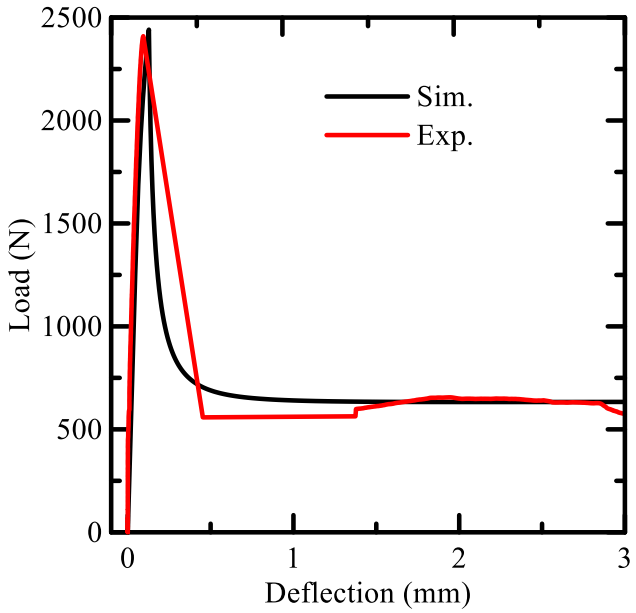
Sim.
Exp.
Load (N)
Deflection (mm)
0
500
1000
1500
2000
2500
0
1
2
3

(b)

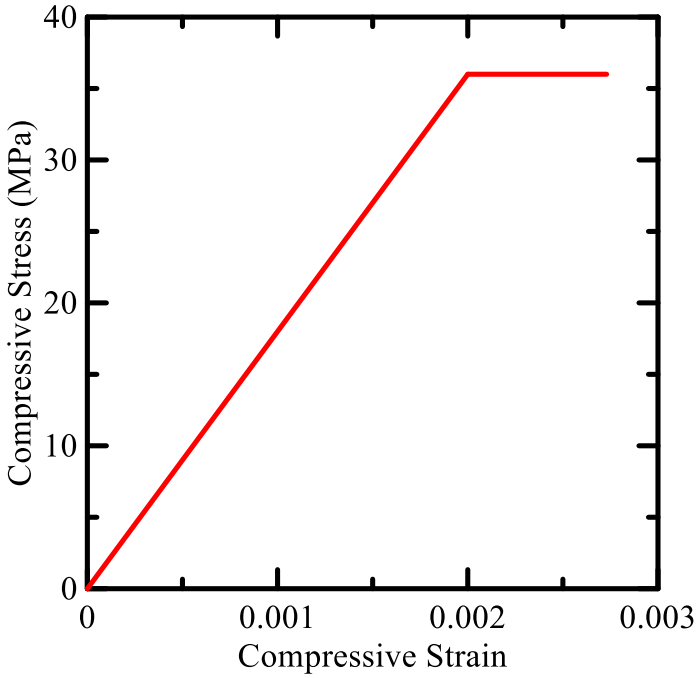
Compressive Stress (MPa)
0
10
20
30
40
0
0.001
0.002
0.003
Compressive Strain

(c)

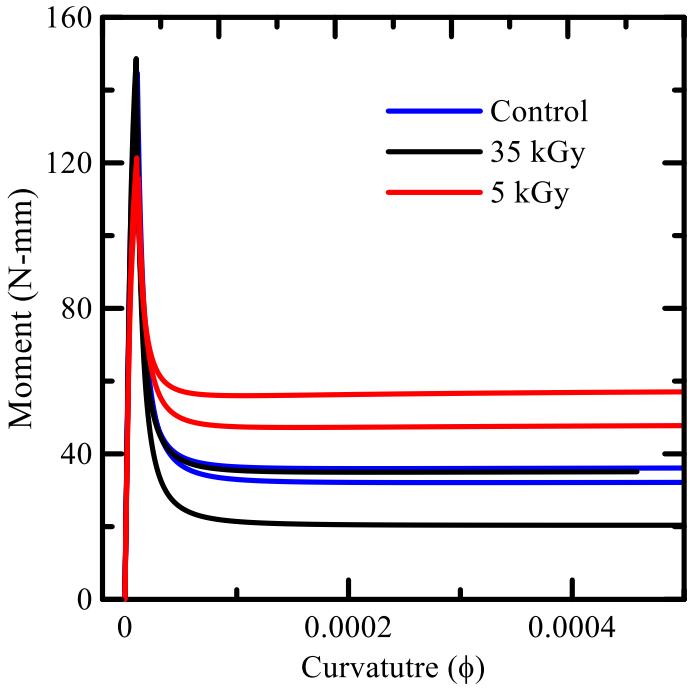
Moment (N-mm)
0
40
80
120
160
0
0.0002
0.0004
Curvatutre (ϕ)
Control
35 kGy
5 kGy

(d)

`

Figure 44: Simulation of results. (a) tensile stress vs strain. (b) Load deflection simulation for a sample. (c) Compressive stress strain model. (d) Moment curvature simulation.

To present the tensile stress strain response a back-calculation process from flexure test is employed. A strain softening tensile model is used to simulate the test data. Bilinear stress strain response was obtained for the sample. It can be observed from Figure 44 (a) that the tensile response has 2 stages. One before peak and one after peak, so in this case the η is less than 0. Stage 1, or the response till the peak tensile strength depends on the mix design and dimension of beam but stage 2 depends on the fiber performance. It can be observed that the response in stage 1 is almost similar. However, in stage 2 the response foe the 5 kGy sample is superior to that of control and 35 kGy sample. Further on Figure 44 (b) represent the load deflection results are simulated by the model to obtain important parameter μ, which also dictated the performances of the sample after first crack.

From the closed parametric equation discussed and tabulated in Table 12, the response show in Figure 44 (d) is derived. It can clearly can be observed that the moment carrying capacity after crack obtained from the closed loop solution for the 5 kGy sample is highest. However, the results of control and 35 kGy sample is comparatively very low, in comparison to 5 kGy sample. For example, for the sample shown in Figure 44 (d), we observe an increase of 75% in the moment carrying capacity for 5 kGy sample in comparison to control sample and 35 kGy sample.

`

With reference to Table 13 it can have observed that the μ values are in 0.08 to range of 0.14 for control sample. After radiation there is an increase in the performance of the sample and it can clearly be observed from the μ values. For the 5 kGy sample the μ values range from 0.18 to as high as 0.48. For 35 kGy the values of μ again dropped to 0.14 to 0.18.

`

Table 13: Back Calculation Parameter

Radiation Dose	Specimen ID	E (MPa)	ε_{cr}	α	β_{tu}	μ
0 kGy (Controlled)	B1	21000	0.000105	4	320	0.14
	B2	21000	0.00012	3	400	0.08
	B3	21000	0.0001	3	250	0.13
	B4	19000	0.0001	4	300	0.13
5 kGy	B1	20000	0.0001	4	400	0.18
	B2	18500	0.0001	4	400	0.21
	B3	17500	0.0001	4	400	0.24
	B4	18500	0.0001	4	350	0.31
	B5	16500	0.000095	5	350	0.48
	B6	18000	0.000095	5	350	0.28
35 kGy	B1	20000	0.0001	4	400	0.18
	B2	21000	0.000105	4	320	0.14
	B3	21000	0.000105	4	300	0.17
	B4	21000	0.00011	4	300	0.15
	B5	20000	0.0001	4	300	0.18

`

5 CONCLUSION AND SUMMARY:

Gamma radiation is an adequate tool for the improvement of the mechanical properties of the Forta fiber. Radiating it with 5 kGy dose, improvement of 14% on the stiffness, and a minimal increase of 6% in the average tensile strength of the sample. But conversely a diminution of 41 and 90% in the tensile strengths was observed, when radiated with 35 kGy and 70 kGy of energy. Thus a notable increase in the mechanical properties of the fiber was observed when radiated with 5 kGy. It was also observed that the pullout response was highly dependent on the mixture design and radiation dose. Control sample exhibited varied response due to fibrillated nature of the fiber. Forta fiber exhibits better bond with cement matrix, mainly when an adequate content of fly ash is used. It was also concluded that the radiation affects the bond between fabric and cement matrix, depending on the radiation energy.

On the same grounds, post peak behavioral response of the flexural beam increased once the fiber are radiated with gamma rays. An increase of 181 % and 62 % in Re3 value for 5 kGy and 35 kGy samples was seen in comparison to controlled sample. Similarly, an increase of 102 % and 64 % in Toughness at 3 mm was observed for 5 kGy and 35 kGy in comparison to controlled sample values.

`

REFERENCES

1 Mobasher, B., and Shah, S. P.,"Test Parameters in Toughness Evaluation of Glass Fiber Reinforced Concrete Panels", *ACI Materials Journal,* Sept-Oct. 1989, pp. 448-458.

2 Frondistouyannas, S., "Flexural Strength Of Concrete With Randomly Oriented Glass Fibers", Magazine of Concrete Research, 29 (100): 142-146 1977.

3 Mobasher, B., and Shah, S. P.,"Test Parameters in Toughness Evaluation of Glass Fiber Reinforced Concrete Panels", *ACI Materials Journal,* Sept-Oct. 1989, pp. 448-458.

4 Mobasher, B. and Li, C. Y., "Mechanical Properties of Hybrid Cement Based Composites," ACI Materials Journal, Vol. 93, No.3, pp.284-293, 1996.

5 EEE 460 Nuclear Power Engineering, retrived November 13, 2015, from http://holbert.faculty.asu.edu/eee460/eee460.html

6 Martin, J.E., Physics for Radiation Protection, WIELY-VCH press, release date: 2012, ISBN:9783527667093

7 Platzer, N.A.J., “Irradiation of poymer” Advances in chemistry , American chemical society, 1967.

8 Machnowski, W., Gutarowska, B, Perkowski, J., Wrzosek, H.“ Effect of gamma radiation on the mechanical properties of and susceptibility to biodegradation of natural fibers” Textile research journal, 2013, 44-55.

9 Grummon, D.S., Schalek, R., Kalantar, J., Dzral, L.T., “High-energy ion implantation of polymeric fibers for modification of reinforcement -matrix adhesion” Nuclear instruments and method in physics research, 1991, 1271-1275.

10 Miao, M., Hawkins, S.C., Cia, J.Y., Gengenbach, T.R., Knott, R., Huynh, C.P., “ Effect of gamma radiation on the mechanical properties of carbon nantube yarns”, Carbon 49, pp 4940-4947, 2011.

11 Borcia, C., Borcia, G., Dumitrascu, N. “ Surface treatment of polymer by plasma and UV radiation,” Rom. Journal Physics, Vol 56, 2011, 224-232.

12 Wu, H.C., Li, V.C. “Fiber/cement interface tailoring with plasma treatment,” Cement and concrete composites, 1999, 205-212.

13 Martínez-Barrera G, Menchaca Campos C, Ureña-Nuñez F, Gamma radiation as a novel technology for the development of new generation concrete. In “Gamma Radiation” (ed.: Feriz Adrovic), InTech: Rijeka Croatia, 91-114, 2012.

`

14 Menchaca-Campos, , Barrera-Díaz C, Martínez-Barrera G and Gencel O, Influence of irradiated polymeric fibers on the mechanical properties of concretes: analysis by microscopy, 2012.

15 Martínez-Barrera G, Martínez-Hernández AL, Velasco-Santos C, Brostow W. Polymer concretes improved by fiber reinforcement and gamma irradiation. e-Polymers 2009; 103: 1-14

16 Martínez-Barrera G, Vigueras-Santiago E, Hernández-López S, Menchaca-Campos C, Brostow W. Mechanical improvement of concrete by irradiated polypropylene fibers. Polym. Eng. Sci. 2001; 45; 1426-1431.

17 Martínez-Barrera G, Martínez-López M, Vigueras-Santiago E, Gencel O, Beycioglu A, João Marciano Laredo dos Reis d. "Polymer concrete reinforced with luffa fibers: effect of gamma radiation" Rev. Tec. Ing. Uni. Zulia. Vol 37 (2007), 22-29.

18 Kaewtatip.K, Thongmee. "Studies of structure and properties of thermoplastic starch/Luffa fiber composites, Material and design 40, 314-318, 2012.

19 ICONTEC, Explorando el concreto reforzado con fibras CRF, Noticreto 2007; 1(84).

20 Cataño L, Albano C, Karam A, Domínguez N, Sánchez Y, González J, Effect of gamma irradiation on mechanical, thermal and rheological behavior of HDPE filled with seaweed residues. Nuclear Instruments and Methods in Physics Research Section B 2005; 236 (1-4): 348-353.

21 Martínez-Barrera G., Martínez-Hernández, A. L., Velasco-Santos, C., Martínez-Lópeza, M., Ortiz-Espinoza J., and Marciano Laredo dos Reis J. "Polypropylene Fibre Reinforced Polymer Concrete: Effect of Gamma Irradiation", Polymer &Polymer Composites, Vol. 22 (2014) , No. 9.

22 Reis J.M.L., *Materials Research*, (12) 63-67.

23 Abd El-Latif, A.A., Ikraiam, F.A., Elazziz, A.Abd, Jamila, "Effect of Gamma Ray Energies Ans Steel Fiber Addition by weight on some shielding properties of Limestone Concrete", 4th Environmental Physics Conference, March 2010, pp. 123-132.

24 Bobadilla-Sancez E, Martinez-Barrera G, Brostow W, Datasshvili. T " Effect of polyester fiber and gamma irradiation on mechanical properties of polymer concrete containing CaCO3 and silica sand" Express Polymer Letters Vol. 3, No. 10 (2009) 615-620.

25 Gamma irradiator for radiation process, IAEA, 2005.

`

26 Aveston, J. Cooper, G. A. and Kelly, A. " Single and Multiple Fracture "; pp.15-26 in The Properties of Fiber Composites, PC Science and Technology Press (1971).

27 Kelly, A., and Tyson W. R. (1965). "Fiber-strengthened materials." Proc., High-Strength Materials ; Proceedings of the Second Berkeley International Materials Conference: High-Strength Materials – Present Status and Anticipated Developments, Berkeley, CA., 578-602.

28 Bennison, S.J., Lawn, B.R. (1989) "Role of Interfacial Grain-Bridging Sliding Friction in the Crack-Resistance and Strength Properties of Non-Transforming Ceramics", Acta Metall., Vol. 37, No. 10, pp. 2659-2671.

29 Cox , B. N. (1993) "Scaling for Bridged Cracks," Mech. of Matls, 15, 87-98.

30 McCartney, L. N. (1987) "Mechanics of Matrix Cracking in Brittle-Matrix Fiber Reinforced Composites," Proc., R. Soc. London, A409, pp. 329-350

31 Budiansky, B., Hutchinson, J.W., and Evans, A.G. (1986) "Matrix Fracture in Fiber Reinforced Ceramics," J. of Mech. and Phy. Solids, V. 343, No. 2, pp. 167-189.

32 Marshall, D. B., Cox, B. N., and Evans, A. G. (1985) "The Mechanics of Matrix Cracking in Brittle Matrix Fiber Composites," Acta Metal,V.33, No.11, pp. 2013-2021.

33 Stang, H., Li, Z. and Shah, S.P., "Pullout Problem: Stress versus Fracture Mechanical Approach," *Journal of Engineering Mechanics*, Vol.116, No.10, 1990, pp.2136-2149.

34 Naaman, A.E., Namur, G.G., Alwan, J.M. and Najm, H.S., "Fiber Pull-out and Bond Slip. I: Analytical Study. II: Experimental validation." *Journal of Structural Engineering*, Vol.117, No. 9, 1991, pp.2769-2800.

35 Sujivorakul, C., Waas, M. and Naaman A.E., "Pullout Response of a Smooth Fiber with an End Anchorage," *Journal of Engineering Mechanics*, Vol.126, No.9, 2000, pp.986-993.

36 Abrishami, H.H. and Mitchell, D., "Analysis of Bond Stress Distributions in Pull-out Specimens," *Journal of Structural Engineering*, Vol.122, No.3, 1996, pp.255-261.

37 Focacci, F., Nanni, A. and Bakis, C.E., "Local Bond Slip Relationship for FRP Reinforcement in Concrete," *Journal of Composites for Construction*, Vol.4, No. Feb., 2000, pp.24-32.

38 Marshall, D.B. (1992) "Analysis of Fiber Debonding and Sliding Experiments in Brittle Matrix Composites," Acta, Metall. Mater, Vol 40., No. 3, pp. 427-441.

39 Marshall, D. B. and Oliver, W. C. (1987) "Measurement of Interfacial Mechanical Properties in Fiber Reinforced Ceramic Composites", J. Am. Ceram. Soc., 70(8), 542-548.

40 Hsueh, C.H. (1990a) "Interfacial friction analysis for fiber-reinforced composites during fiber push-down (indentation)", J. Material Science, 25, 818-828

41 Hsueh, C.H.,(1990b)"Interfacial Debonding and Fiber Pullout Stresses of Fiber Reinforced Composites," Materials Science and Engineering, A123, pp1-11.

42 Hutchinson, J.W., and Jensen, H.M. (1990) "Models of Fiber Debonding and Pullout in Brittle Composites with Friction", Mech. of Matls., 9, 139-163.

43 Cox, B.N. (1990), Acta Metall. mater. 38, 2411.

44 Dollar, A., and Steif, P.S. (1993) "Analysis of the Fiber Push-out Test," Int. J. Solids Struc., Vol. 30, No. 10, pp 1313-1329.

45 Ballarini, R., Ahmed, S., and Mullen, R. L. (1990) "Finite Element Modeling of Frictionally Restrained Composite Interfaces," Interfaces in Metal-Ceramic Composites, Proc. of the Int. Conf. on Interfaces in Metal Ceramics Comp., Feb. 18-22, pp 349-388.

46 Mital, S. K., and Chamis, C.C.,(1990) "Fiber Pushout Test: A Three Dimensional Finite Element Computational Simulation," Journal of Composite Technology & Research, JCTRER, Vol. 13, No. 1, pp. 14-21.

47 Li, Z., Mobasher, B., and Shah, S. P. (1991) "Characterization of Interfacial Properties of Fiber Reinforced Cementitious Composites," J. of Am. Ceram. Soc., 74(9) pp. 2156-64.

48 Mobasher B., Cheng Yu Li, "Effect of Interfacial Properties on the Crack Propagation in Cementitious Composites," Advanced Cement Based Materials, 1996;4, pp. 93-105

49 Purnell, P., Buchanan, A.J., Short, N.R., Page, C.L., Majumdar, A.J., "Determination of bond strength in glass fibre reinforced cement using petrography and image analysis," Journal of Materials Science, 35 (18): 4653-4659 SEP 2000.

`

50 Naaman, E. A., Namur, G. G., Alwan, J. M., and Najm, H. S. (1991a). "Fiber Pullout and Bond Slip. I: Analytical Study." *J. of Structural Eng.*, 117, 2769-2790.

51 Naaman, E. A., Namur, G. G. Alwan, J. M. and Najm, H. S. (1991b). "Fiber Pullout and Bond Slip. II: Experimental Validation" *J. of Structural Eng.*, 117, 2791-2800.

52 Vandewalle, L. et al., "Test and design methods for steel fiber reinforced concrete: Recommendations for σ-ε design method," *Materials and Structures*, Vol. 33, No. 226, 2000, pp. 75-81.

53 Soranakom, C., and Mobasher, B., "Closed-Form Moment-Curvature Expressions For Homogenized Fiber Reinforced Concrete," *ACI Material Journal*, Vol. 104, No. 4, July-August, 2007, pp. 351-359.

54 Chuang T.-J., and Mai, Y.-W., "Flexural Behavior of Strain-Softening Solids," *Int. J. Solid Structures*, Vol. 25 No. 12, 1989, pp. 1427-1443.

55 Wee, T.H., and Lu, H.R., and Swaddiwudhipong S., "Tensile Strain Capacity of Concrete under Various States of Stress," *Magazine of Concrete Research*, Vol. 52, No. 3, June 2000, pp. 185-193.

`

APPENDIX

A EXPERIMENTAL AND MISCELLANEOUS RESULTS

`

Fiber tension data

1. Diametric Calculation of Fiber by optical microscope approach:

   Due to fibrillated nature of the fiber it is difficult to consider the cross section of the fiber as circular and even it was physically not possible to calculate the diameter of a single filament with Vernier or scale. Optical Microscope was used for this purpose. However, the procedure to calculate the diameter accurately and eliminate the errors is explained below:

   1. Take a single strand of the fiber.
   2. Take a rectangular box or mold.
   3. Put masking tape at the end of it and then with a razor put a small hole in the middle, pass the fiber through, and pinch the masking tape to close.
   4. Now pull the fiber tight and mix 4-5 cc of the epotek.
   5. Pore fluorescent dye in the mold and vacuum it to remove all the air.
   6. The shape of the single yarn cross section is approximated to an elliptical shape and the length of semi major and minor axis can be determined.

      Cross Sectional Area of an Ellipse: πab

      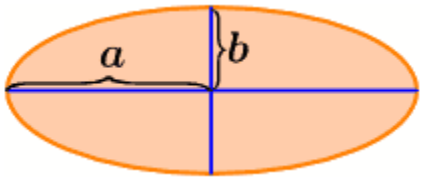

   7. Multiple measurement will be taken to provide higher accuracy in geometric measurement.

`

Area of ellipse:

a	b	Area
201.5μm	93.5 μm	0.0591 μm^2

Approximate Diameter of a single filament:

$$\frac{\pi}{4} D^2 = 0.0591 \mu m^2 \quad 3.1$$

$D = 2.743 * 10^{-4} m = 0.27431 mm (0.0108 inches)$

For two filaments:

$D = 3.88 * 10^{-4} m = 0.388 mm (0.01527 inches)$

`

Optical Microscopes images:

a.

b.

`

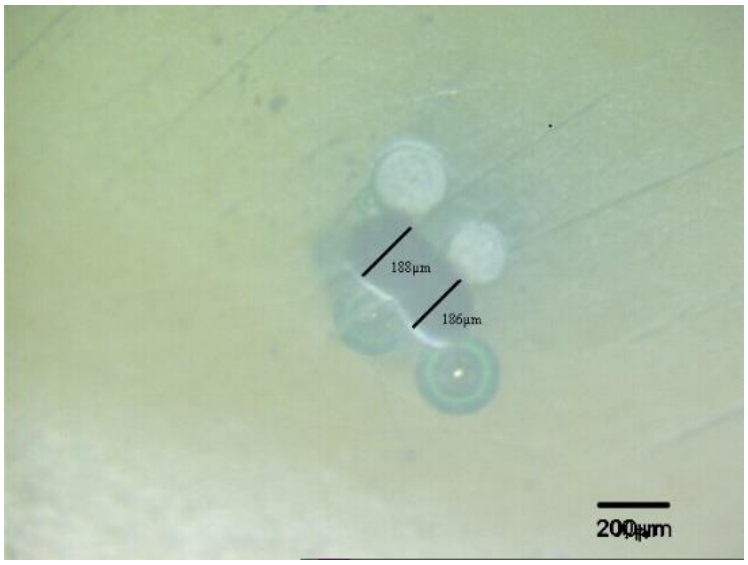

c.

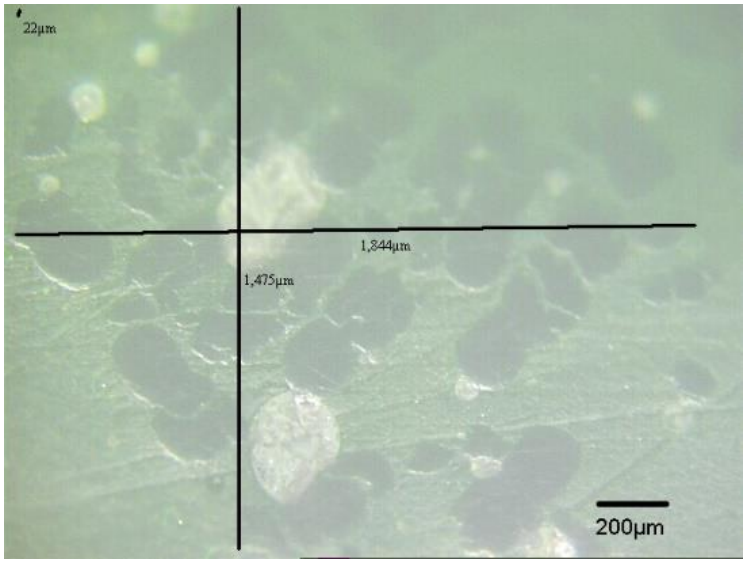

d.

Figure A- 1: Optical Microscopic images. (a) Optical microscopic specimen. (b) x axis measurement of a single test filament. (c) Y axis measurement of single test filament. (d) axis measurement of the whole bundle.

`

2. Flexure Beam Mix Design:

Beam Sizes: 2" x 2.5" x 14" aggregate /total cement = 2

No. of Beams: 6 w/c = 0.42

Total Quantity: 0.243 cubic ft.

Add 30%: 0.315 cubic ft.

Table A-1: Mix Design Table.

%	Material	SG	abs vol.	weight (gms)	weight (lbs)	Final Wt (gms)
85	cement	3.15	0.06	4970.76	10.97	4984.83
15	fly ash	2.17	0.01	877.19	1.94	879.68
0	silica fume	0.7	0.00	0.00	0.00	0.00
	total cement			5847.95	12.90	5864.51
	water	1	0.09	2456.14	5.42	2463.09
100	Fine Aggregate	2.6	0.16	11695.91	25.80	11729.02
	total aggregates			11695.91		

`

Fiber Quantity: 0.5% of the total volume

$= (5/100)*0.32=0.0016\ ft^3$

Weight Calculation:

S.G (Forta Fiber) =0.9.

Weight (Fiber) = 0.9 *1000*0.26*(1000/35.31)

= 40.78 gms ≈ 41 gms

Fibers are fibrillated and are available in bundle. Fibers are cuts to an approximate length of 1 inch and then mixed in the concrete mix

`

Table A-2: Summary of the calculated parameters of the flexural test.

adiation Energy	Specimen ID	Peak Load (kN)	MOR (MPa)	Load at 0.75 mm (L/600) (kN)	Residual Stress at 0.75 mm (L/600) (MPa)	Toughness at 0.75 mm (L/600)(J)	Load at 3 mm (L/150) (kN)	Residual Stress at 3 mm (L/150) (MPa)	Toughness at 3 mm (L/150) (J)	Equivalent Flexural Strength at 3 mm, Re_3 (%)
0 kGy (Controlled)	B1	2.58	5.6	2.4	5.31	0.13	0.54	1.17	0.96	15.7
	B2	2.4	5.3	0.09	0.2	0.31	0.09	0.2	0.5	8.6
	B3	2.1	4.7	0.03	0.06	0.23	0.33	0.71	0.35	6.83
	B4	1.94	4.2	0.09	0.2	0.52	0.34	0.74	0.93	20.2
	B5	2.34	5.07	0.17	LDVT slipped					
	B6	2.3	5.05	1.97	**					
Average		2.28	4.99	0.79	1.44	0.3	0.33	0.71	0.69	12.83
Std. Dev.		0.23	0.49	1.09	2.58	0.17	0.18	0.4	0.31	6.23
5 kGy	B1	2.17	4.71	1.97	4.28	0.11	0.6	1.21	1.12	21.8
	B2	1.92	4.17	1.89	4.1	0.1	0.64	1.38	1.19	26.1
	B3	1.77	3.85	0.643	1.4	0.64	0.71	1.54	1.5	35.4
	B4	1.91	4.15	1.89	4.1	0.11	0.93	2	1.56	34.5
	B5	1.66	3.6	0.94	2	0.54	1.24	2.7	1.24	66.2

`

	B6	1.93	4.2	0.627	1.36	0.6	0.8	1.73	1.5	32.7
Average		1.9	4.1	1.3	2.9	0.4	0.8	1.8	1.4	36.1
Std. Dev.		0.17	0.37	0.66	1.43	0.27	0.24	0.54	0.19	15.7
35 kGy	B1	2.36	5.14	LDVT slipped						
	B2	2.46	5.34	2.43	5.29	0.13	0.37	0.81	0.6	10.3
	B3	2.4	5.22	0.55	1.21	0.68	0.64	1.4	1.64	28.7
	B4	2.53	5.5	0.585	1.27	0.19	0.57	1.25	1.16	19.3
	B5	2.09	4.53	2.03	4.42	0.11	0.58	1.27	0.97	19.7
	B6	2.12	4.61	0.45	0.98	0.5	0.64	1.38	1.31	26.1
Average		2.32	5.04	1.2	2.6	0.322	0.56	1.2	1.13	20.82
Std. Dev.		0.2	0.44	0.94	2.05	0.25	0.11	0.24	0.39	7.15

*** Due to crack, there is a leap in the result at this point and thus, this value is out of range.

3. SEM Cross section Images for different irradiation:

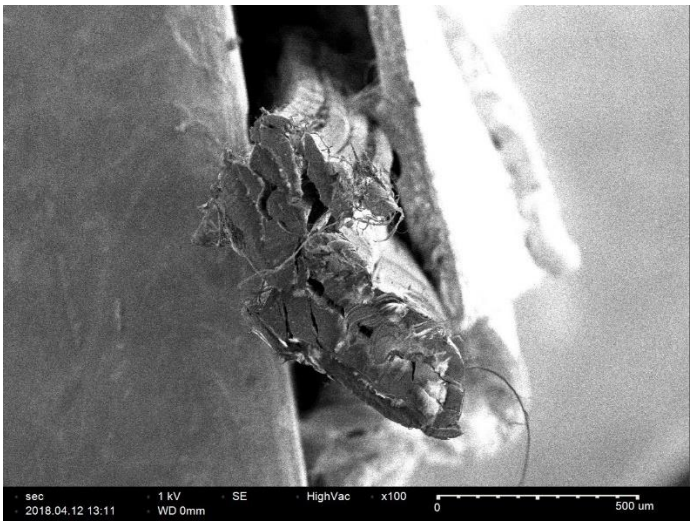

(a)

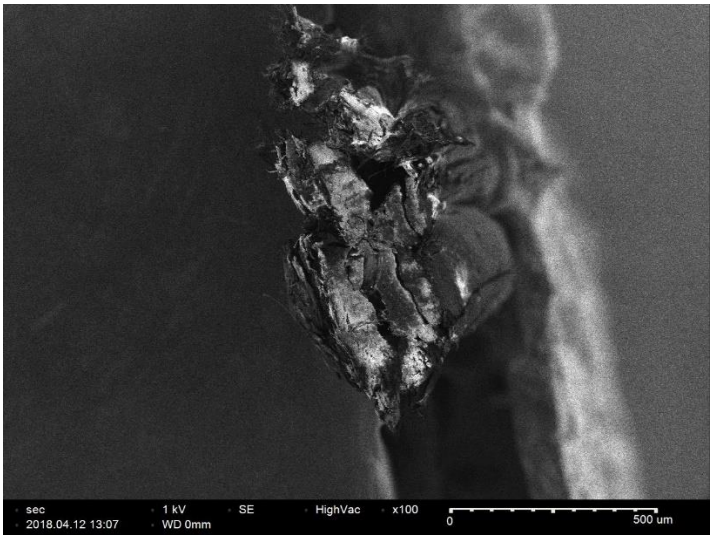

(b)

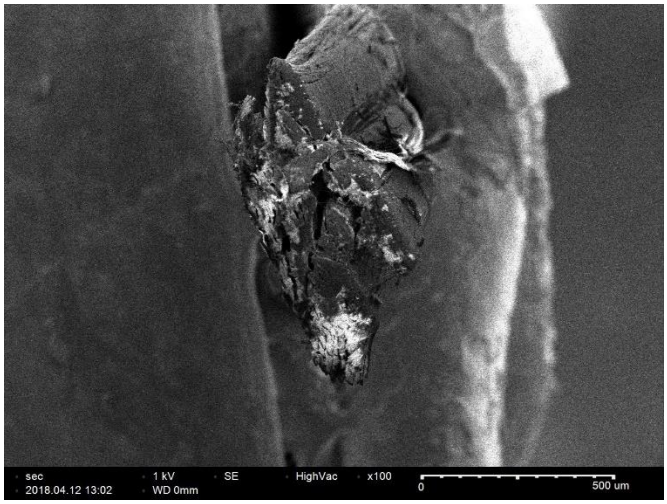

(c)

Figure A- 2: SEM Cross-section Images. (a) 5 kGy (b) 35 kGy (c) 70 kGy